HHS Public Access

Author manuscript

Cancer Cell. Author manuscript; available in PMC 2019 November 12.

Published in final edited form as:

Cancer Cell. 2018 November 12; 34(5): 741–756.e8. doi:10.1016/j.ccell.2018.10.008.

JARID2 Functions as a Tumor Suppressor in Myeloid Neoplasms by Repressing Self-Renewal in Hematopoietic Progenitor Cells

Hamza Celik[1], **Won Kyun Koh**[1], **Ashley C. Kramer**[1], **Elizabeth L. Ostrander**[1], **Cates Mallaney**[1], **Daniel A.C. Fisher**[2], **Jingyu Xiang**[1], **William C. Wilson**[1], **Andrew Martens**[1], **Alok Kothari**[3], **Gregory Fishberger**[1], **Eric Tycksen**[4], **Darja Karpova**[1], **Eric J. Duncavage**[5], **Youngsook Lee**[6], **Stephen T. Oh**[2], and **Grant A. Challen**[1,7,*]

[1]Division of Oncology, Department of Medicine, Washington University School of Medicine, St Louis, MO 63110, USA.

[2]Division of Hematology, Department of Medicine, Washington University School of Medicine, St Louis, MO 63110, USA.

[3]Department of Pediatrics, Washington University School of Medicine, St Louis, MO 63110, USA.

[4]Genome Technology Access Center, Department of Genetics, Washington University in St. Louis, St. Louis, MO 63110, USA.

[5]Department of Pathology & Immunology, Washington University School of Medicine, St Louis, MO 63110, USA.

[6]Department of Cell and Regenerative Biology, University of Wisconsin-Madison, Madison, WI 53705, USA

[7]Developmental, Regenerative and Stem Cell Biology Program, Division of Biology and Biomedical Sciences, Washington University School of Medicine, St Louis, MO 63110, USA.

SUMMARY

[*]Corresponding author and lead contact: Grant A. Challen, Ph.D., Washington Univeristy School of Medicine, Ph: +1 314-362-0987, gchallen@dom.wustl.edu.

AUTHOR CONTRIBUTIONS

Conceptualization: HC, GAC
Methodology: HC, ACK, AM, YL, JX, GAC
Software: HC, ELO, ET
Validation: HC, ELO, EJD, GAC
Formal analysis: HC, ELO, GAC
Investigation: HC, WKK, ACK, CM, WCW, AK, GF, DAF, DK, GAC
Resources: HC, ELO, ET, YL, DAF, STO, GAC
Data curation: HC, ELO, ET
Writing – original draft preparation: HC, GAC
Writing – review and editing: GAC
Visualization: HC, ELO, WCW, GAC
Supervision: GAC
Project administration: GAC Funding acquisition: HC, GAC

How specific genetic lesions contribute to transformation of non-malignant myeloproliferative neoplasms (MPN) and myelodysplastic syndromes (MDS) to secondary acute myeloid leukemia (sAML) are poorly understood. *JARID2* is lost by chromosomal deletions in a proportion of MPN/MDS cases that progress to sAML. In this study, genetic mouse models and patient-derived xenografts demonstrated that JARID2 acts as a tumor suppressor in chronic myeloid disorders. Genetic deletion of *Jarid2* either reduced overall survival of animals with MPN or drove transformation to sAML, depending on the timing and context of co-operating mutations. Mechanistically, JARID2 recruits PRC2 to epigenetically repress self-renewal pathways in hematopoietic progenitor cells. These studies establish JARID2 as a *bona fide* hematopoietic tumor suppressor and highlight potential therapeutic targets.

Graphic Abstract

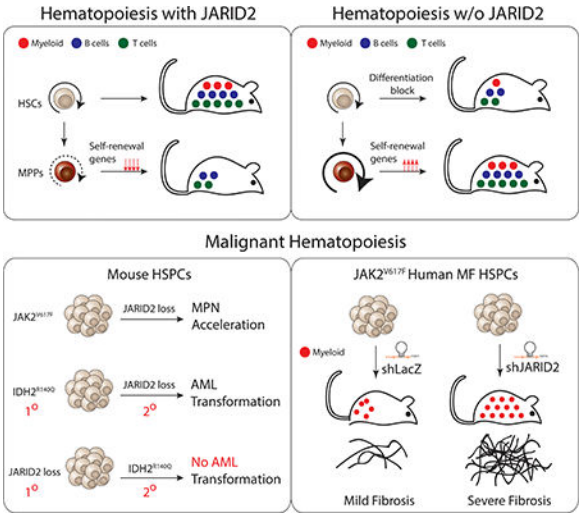

INTRODUCTION

Myeloproliferative neoplasms (MPN) and myelodysplastic syndromes (MDS) are chronic blood disorders driven by genetic mutations in hematopoietic stem cells (HSCs). While these diseases are associated with significant morbidity and mortality, in a substantial portion of patients disease progression leads to transformation to secondary acute myeloid leukemia (sAML). sAML patients have a poor prognosis with average survival time of less than six months (Abdulkarim et al., 2009; Cervantes et al., 1991; Mesa et al., 2005; Passamonti et al., 2005). No efficient therapy exists for post-MPN/MDS sAML, and the mechanisms of transformation remain unclear.

Although genomic studies have identified mutations that contribute to malignant progression of MPN and MDS (Rampal et al., 2014; Tallarico and Odenike, 2015; Walter et al., 2012), the functional contribution of these events to disease pathogenesis largely remains to be determined. The clonal evolution of MPN and MDS to sAML is driven by acquisition of cooperating mutations. Recent studies have identified deletions of *JARID2*, encoding a co-factor of Polycomb Repressive Complex 2 (PRC2), in up to 6.5% of post-MPN/MDS sAML (Milosevic et al., 2012; Puda et al., 2012). These chromosomal deletions are heterozygous

involving the short arm of chromosome 6 and delete all *JARID2* (Puda et al., 2012). Deletions of *JARID2* are restricted to the sAML phase of disease (Puda et al., 2012; Rampal et al., 2014) and are not reported in *de novo* AML (Cancer Genome Atlas Research et al., 2013). Thus, *JARID2* deletion could be a sAML-specific transforming event, and JARID2 may function as a hematopoietic tumor suppressor.

Polycomb repressive complexes are epigenetic regulators that control multiple aspects of stem cell fate. PRC2 consists of three core subunits: Suz12, Eed and Ezh2, and is responsible for the establishment of repressive chromatin marks histone H3 lysine 27 di-/trimethylation (H3K27me2/3) (Cao et al., 2002). Mouse models have shown that alterations to PRC2 can have catastrophic consequences for hematopoiesis (Lee et al., 2015; MochizukiKashio et al., 2011; Xie et al., 2014). While the importance of core PRC2 components in hematopoiesis is established, the function of PRC2 co-factors such as JARID2 remains almost completely unknown. In this study, we examined the role of JARID2 in normal and malignant hematopoiesis.

RESULTS

JARID2 is a Hematopoietic Tumor Suppressor

We generated an inducible genetic model by crossing mice in which exon three of *Jarid2* is floxed (Mysliwiec et al., 2006) to the Mx1-CRE strain (Kuhn et al., 1995). Activation of Mx1CRE by polyinosinic:polycytidylic acid (pIpC) facilitated effective recombination in HSCs (Figure S1A) and protein ablation (Figure S1B). To mirror genetic progression observed in patients, c-Kit^{+} bone marrow (BM) progenitors from Mx1-CRE:*Jarid2*$^{+/+}$ (Control^{Mx1}) and Mx1-CRE:*Jarid2*$^{fl/fl}$(*Jarid2*-KO^{Mx1}) mice (pre-pIpC) were transduced with a lentivirus expressing IDH2^{R140Q} (and GFP; Figure S1C) and transplanted into recipient mice. *IDH2*^{R140Q} mutations are reported in patients preceding *JARID2*-deleted sAML (Rampal et al., 2014). Approximately 4% of floxed alleles were recombined prior to pIpC due to non-specific activity of Mx1-CRE, and transduction increased this to 8% (Figure S1D). Recipients were treated with pIpC eight weeks posttransplant. GFP^{+} cell chimerism in the blood of mice transplanted with IDH2^{R140Q}:*Jarid2*-KO^{Mx1} cells increased significantly compared to the control group (Figure 1A), suggesting deletion of *Jarid2* provided IDH2^{R140Q}-expressing cells a competitive advantage. Although there was no difference in overall survival in primary recipients (Figure 1B), IDH2^{R140Q}:*Jarid2*-KO^{Mx1} recipient mice developed splenomegaly, leukocytosis and neutrophilia (Figure 1C) and succumbed to AML (>20% blasts in the BM (Kogan et al., 2002); Figure 1D) whereas recipients of IDH2^{R140Q}:Control^{Mx1} cells developed a myeloproliferative (MPD) disorder. Transfer of 1×10^{6} BM cells from primary IDH2^{R140Q}:*Jarid2*-KO^{Mx1} implanted mice to secondary recipients resulted in 100% AML penetrance (median survival = 27-days, Figure 1E) with splenomegaly and leukocytosis (Figure 1F). Flow cytometric analysis identified rampant leukemic cells (GFP^{+} Lineage^{-} c-Kit^{+} FCÛRII/III^{+}; Figure 1G) in the spleen and BM (Figure 1H).

To determine the impact of mutation order, IDH2^{R140Q} was introduced into Control^{Mx1} and *Jarid2*-KO^{Mx1} c-Kit^{+} cells eight weeks post-pIpC. There was no advantage for IDH2^{R140Q}expressing cells in a pre-deleted *Jarid2* background (Figure 1I). While overall

survival of recipient mice was again reduced in the absence of *Jarid2* (Figure 1J), there was no evidence of leukemic progression (Figure 1K). Although deletion of *Jarid2* did confer long-term engraftment to IDH2^{R140Q}-expressing cells in secondary recipients (Figure 1L), no mice developed hematological disease (Figure S1E). The only colony-forming potential within the GFP^{+} BM fraction was possessed by the IDH2^{R140Q}:*Jarid2*-KO^{Mx1} combination (Figure S1F). These data establish two key points; (1) JARID2 is a *bona fide* hematopoietic tumor suppressor, and (2) the mutational order of *Jarid2* deletion is critical for leukemic transformation.

Loss of JARID2 Leads to Depletion of Primitive Hematopoietic Progenitors

To understand how JARID2 functions as a tumor suppressor, we sought to elucidate its role in normal hematopoietic development by crossing *Jarid2*$^{fl/fl}$ mice to the Vav-CRE strain (Georgiades et al., 2002) (Figure S2A,B). Analysis of 10 week old mice revealed that despite an overall increase in BM cellularity in Vav-CRE:*Jarid2*$^{fl/fl}$ mice (*Jarid2*-KO^{Vav};Figure S2C), there was a significant reduction of phenotypically-defined HSCs (Lineage^{-}c-Kit^{+}Sca-1^{+}CD48^{-}CD150^{+}) and multipotent progenitors (MPPs; Lineage^{-}c-Kit^{+}Sca-1^{+}CD48^{-}CD150^{-}; Figure 2A,B). A similar phenotype was observed in *Jarid2*-KO^{Mx1} mice eight weeks post-pIpC treatment of eight week old mice (Figure S2D). To confirm the reduction in HSCs was not due to alteration of immunophenotype, side population (SP) staining (Goodell et al., 1996) was performed. There was a three-fold reduction in SP in the absence of *Jarid2* (Figure S2E,F). The reduction of HSCs and MPPs in *Jarid2*-KO^{Vav} mice was not due to differences in apoptosis (Figure 2C). While there were no differences in cell cycle in HSCs, *Jarid2*-KO^{Vav} MPPs were significantly less quiescent than Vav-CRE:*Jarid2*$^{+/+}$ (Control^{Vav}) and Vav-CRE:*Jarid2*$^{fl/+}$ (*Jarid2*-HET^{Vav}) MPPs (Figure 2D,E). To force quiescent HSCs to divide, mice were treated with 5-flurouracil (5-FU) and labelled with BrdU for 96 hr. Despite no differences in cell cycle under basal conditions, significantly fewer *Jarid2*-KO^{Vav} HSCs incorporated BrdU in response to 5-FU challenge (Figure 2F), suggesting they are less able to exit quiescence in response to proliferative stress.

Blood analysis revealed peripheral cytopenias (Figure S2G), and a shift towards T cell differentiation at the expense of B cells (Figure S2H) in *Jarid2*-KO^{Vav} mice. This was consistent with reduced B lineage progenitors in the BM of *Jarid2*-KO^{Vav} mice (Figure S2I), and an accumulation of double negative 2 progenitors and increased single positive T-cells in the thymus (Figure S2J). No differences in myeloid progenitors were noted in young mice (Figure S2K). A cohort of mice were monitored for 550 days of age (Figure 2G). 62.5% (10/16) of *Jarid2*-KO^{Vav} mice became morbid in this timeframe (median survival = 473-days). One mouse developed malignant lymphoma, and 2/10 mice succumbed to infections from opportunistic bacteria. The remaining 7/10 mice developed nonreactive myeloid proliferation characterized by BM hypercellularity, splenomegaly, increased myeloid cells in the BM and blood (Figure 2H) and increased myeloid progenitors in the BM (Figure S2L). The depletion of HSCs and MPPs observed in young *Jarid2*-KO^{Vav} mice was exacerbated in aged mice (Figure 2I). *Jarid2*-HET^{Vav} mice showed similar phenotypes with longer latency, including osteopetrotic trabecular bone formation with focal reticulin fibrosis (Figure 2J). These pathologies were most consistent with a diagnosis of MPD/MPN.

HSCs Lacking JARID2 Have Defective Differentiation

To examine consequences of *Jarid2* deletion on HSC function, transplantation assays were performed. Limiting dilution whole bone marrow (WBM) transplants showed no difference in long-term multi-lineage repopulation (LTMR; >1% chimerism of donor-derived cells to myeloid, B cell and T cell blood lineages at 16 weeks post-transplant; Figure S3A) between ten week old Control^{Vav} and *Jarid2*-KO^{Vav} mice (Figure S3B,C). Transplantation of 2.5×10^5 WBM from 16 week old *Jarid2*-KO^{Mx1} mice (eight weeks post-pIpC treatment) against 2.5×10^5 WBM wild-type competitor showed no difference in engraftment (Figure 3A) or lineage chimerism (Figure 3B). Secondary transfer of 3×10^6 WBM cells from primary recipients showed no difference in total blood engraftment (Figure 3C), but a bias towards myeloid cell generation at the expense of B cells from *Jarid2*-KO^{Mx1} BM (Figure 3D). 100 purified HSCs from Control^{Mx1} and *Jarid2*-KO^{Mx1} mice were transplanted along with 2.5×10^5 WBM competitor cells. Again there was little difference in engraftment (Figure 3E) or lineage chimerism (Figure S3D) in primary recipients. To stringently assess HSC self-renewal, at 18 weeks post-transplant 100 donorderived HSCs (CD45.2$^+$Lineage$^-$c-Kit$^+$Sca-1$^+$CD48$^-$CD150$^+$) were re-purified from primary recipients and transplanted into secondary recipients. In this setting, *Jarid2*-KO^{Mx1} HSCs failed to contribute to blood (Figure 3F). BM analysis 18 weeks post-transplant showed frequency of donor-derived HSCs was similar in recipients of HSCs from the different genotypes (Figure 3G,H), suggesting self-renewal of *Jarid2*-KO^{Mx1} was intact but differentiation was impaired. Analogous results were obtained from competitive transplantation of 100 HSCs isolated from ten-week old Control^{Vav} and *Jarid2*-KO^{Vav} mice, but the phenotype was more severe with an engraftment deficit evident in primary transplants (Figure 3I), and a complete dearth of donorderived blood in secondary recipients (Figure 3J). But again, BM analysis showed self-renewal of *Jarid2*-KO^{Vav} HSCs was not compromised (Figure 3K, Figure S3E).

We postulated the difference in primary transplant output between *Jarid2*-KO^{Vav} and *Jarid2*-KO^{Mx1} HSCs was due to the duration of *Jarid2* deletion from the different CRE models. To test this, we performed competitive transplantation using 100 HSCs purified from 14 month old *Jarid2*-KO^{Mx1} and Control^{Mx1} donor mice (12 months post-pIpC). This transplant replicated the *Jarid2*-KO^{Vav} results with no peripheral blood contribution from old *Jarid2*-KO^{Mx1} HSCs (Figure 3L). The persistence of *Jarid2*-KO HSCs in the BM of transplant recipients without corresponding contribution to peripheral blood suggested that differentiation was defective in *Jarid2*-KO HSCs, or *Jarid2*-KO HSCs are unable to escape quiescence. To test the latter, BM chimeras were established by transplanting mice with 5.0×10^5 WBM cells from Control^{Vav} or *Jarid2*-KO^{Vav} mice along with 5.0×10^5 WBM from wild-type mice. Eight weeks post-transplant, chimeras were treated with serial injections of 5-FU. Survival of *Jarid2*-KO^{Vav} chimeras was significantly compromised (Figure 3M). Proliferation analysis following one dose of 5-FU revealed significantly fewer BrdU$^+$ *Jarid2*-KO^{Vav} HSCs (Figure 3N,O). These data suggest that HSC proliferation and differentiation is impaired in the absence of *Jarid2*.

JARID2 Restricts Self-Renewal in Multipotent Progenitors

The contrast between transplantation of WBM versus HSCs suggested that a population of cells other than HSCs may contribute to hematopoietic regeneration in the absence of *Jarid2*.

To ascertain this cell fraction, we performed competitive transplantation of 250 restricted progenitors (RPs; Lineage$^-$c-Kit$^+$Sca-1$^+$CD48$^+$CD150$^-$) and 100 MPPs. RPs from Control^{Vav} and *Jarid2*-KO^{Vav} mice (Figure S4A) did not exhibit long-term engraftment (Figure S4B,C). Control^{Vav} MPPs were unable to sustain tri-lineage hematopoiesis (Figure 4A). Surprisingly, *Jarid2*-KO^{Vav} MPPs were able to reconstitute tri-lineage hematopoiesis effectively over 16 weeks (Figure 4A,B). In contrast to Control^{Vav} MPPs, *Jarid2*-KO^{Vav} MPPs showed significant contribution to long-term myelopoiesis (Figure 4C), an indicator of active hematopoietic output. To assess self-renewal of *Jarid2*-KO^{Vav} MPPs, 18 weeks post-transplant 3×10^6 WBM cells or 100 donor-derived MPPs (CD45.2$^+$Lineage$^-$c-Kit$^+$Sca-1$^+$CD48$^-$CD150$^-$) from primary recipients were re-purified and transplanted into secondary mice. *Jarid2*-KO^{Vav} MPPs were able to reconstitute secondary recipients with robust tri-lineage hematopoiesis (Figure 4D, S4D). No engraftment was observed from Control^{Vav} MPP-derived cells in secondary recipients (Figure 4E). Similar results were produced from transplantation of aged *Jarid2*-KO^{Mx1} MPPs (Figure S4E). The engraftment from sorted *Jarid2*-KO^{Vav} MPPs was not due to HSC contamination (Figure S4F). BM analysis revealed a significant increase in the number of MPPs in primary recipients of *Jarid2*-KO^{Vav} MPPs (Figure 4F) which underwent further expansion in secondary recipients (Figure 4G), suggestive of self-renewal. To define the importance of the ontogeny, 100 donor-derived MPPs were re-purified from mice originally transplanted with *Jarid2*-KO^{Vav} HSCs and transplanted into secondary recipients. Unlike *Jarid2*-KO^{Vav} MPPs derived from *Jarid2*-KO^{Vav} MPPs, *Jarid2*-KO^{Vav} MPPs derived from *Jarid2*-KO^{Vav} HSCs were unable to sustain multi-lineage hematopoiesis in secondary recipients (Figure 4H). As another indicator of acquired self-renewal, MPPs from *Jarid2*-HET^{Vav} and *Jarid2*-KO^{Vav} mice showed serial replating capacity *in vitro*, unlike Control^{Vav} MPPs (Figure 4I). To eliminate the possibility that loss of *Jarid2* alters HSC immunophenotype, MPPs were isolated from *Rosa26*$^{Cas9\text{-}GFP}$ mice and transduced with guide RNAs (gRNAs) that target *Jarid2* (Figure S4G). The experiment also included a non-targeting (NT) negative control gRNA, and gRNAs targeting *Ezh2* to determine if the phenotype was dependent on PCR2. *Jarid2*-gRNA targeted *Rosa26*$^{Cas9\text{-}GFP}$ MPPs showed enhanced colony formation *in vitro* (Figure S4H), and long-term engraftment in BM transplantation (Figure 4J), unlike the other gRNA-targeted *Rosa26*$^{Cas9\text{-}GFP}$ MPPs. Thus, deletion of *Jarid2* removes constraints limiting self-renewal in non-HSC progenitors.

JARID2 Collaborates with PRC2 to Regulate Gene Networks that Govern HSC Identity

Co-immunoprecipitation in mouse thymocytes confirmed that JARID2 binds PRC2 (Figure S5A). *Jarid2* knockout 32D cells (murine myeloid progenitor line) showed decreased H3K27me3 (Figure S5B). RNA-seq profiles were generated for Control^{Vav} and *Jarid2*-KO^{Vav} HSCs and MPPs. Gene set enrichment analysis (GSEA) revealed that genes upregulated in *Jarid2*-KO^{Vav} HSCs and MPPs strongly overlap with Ezh2 targets (Lu et al., 2010) (Figure 5A, S5C). Expression of PRC2 components was not altered in *Jarid2*-KO^{Vav} cells. The most significantly downregulated gene set in *Jarid2*-KO^{Vav} HSCs was G_2/M checkpoint progression (Figure 5B), which may be a mechanism contributing to their inability to exit quiescence. 527 genes were differentially expressed (>2-fold, $p<0.01$), between Control^{Vav} HSCs and *Jarid2*KO^{Vav} HSCs (Table S1) of which most were upregulated, consistent with the role of JARID2 as a repressor. Genes upregulated in *Jarid2*-

KO^{Vav} HSCs significantly overlapped with HSC “fingerprint” genes (Chambers et al., 2007), genes expressed specifically in normal HSCs compared to downstream progeny (Figure S5D). The upregulation of HSC-identity genes combined with reduced ability to exit quiescence likely contributes to the differentiation deficit of HSCs lacking *Jarid2*, similar to what has been observed for other epigenetic regulators such as *Dnmt3a* (Challen et al., 2014; Jeong et al., 2018).

We hypothesized the long-term repopulating capacity of *Jarid2*-KO^{Vav} MPPs was at least partly due to the inability to silence self-renewal networks. Genes downregulated in Control^{Vav} MPPs relative to Control^{Vav} HSCs were defined and cross-referenced to genes upregulated (derepressed) in *Jarid2*-KO^{Vav} MPPs compared to Control^{Vav} MPPs. Of the 685 genes downregulated in Control^{Vav} MPPs relative to Control^{Vav} HSCs, 65 genes were not repressed in *Jarid2*-KO^{Vav} MPPs (Figure 5C). 11 of these genes are normally specifically expressed in HSCs (Chambers et al., 2007) (Figure 5D), including the characterized HSC markers *Fgd5* (Gazit et al., 2014) and *Hoxb5* (Chen et al., 2016) (Figure S5E). *Runx1t1* and *Mycn*, which can help reprogram differentiated blood cells to a HSC-like state (Riddell et al., 2014), were de-repressed in *Jarid2*-KO^{Vav} MPPs (Figure 5E). These data suggest that *Jarid2* deletion in MPPs activates gene networks that govern HSC identity.

Jarid2 Deletion is Associated with a Loss of H3K27me3 in Gene Bodies

ChIP-mentation (Schmidl et al., 2015) was performed to examine whether increased expression of HSC-identity genes in *Jarid2*-KO^{Vav} HSCs and MPPs was associated with changes in H3K27me3. Genotype was a more powerful correlative of H3K27me3 than cell identity (Figure S5F). H3K27me3 changes (>1.7-fold, $p<0.01$) were concentrated upstream of transcriptional start sites and introns in *Jarid2*-KO^{Vav} HSCs and MPPs (Figure 5F). For many HSC-identity genes upregulated in *Jarid2*-KO^{Vav} HSCs and MPPs such as *Mycn*, *Runx1t1*, *Fgd5* and *Vdr*, H3K27me3 depletion was observed across gene bodies (Figure 5G, S5G). This effect was specific to this set of genes as a global correlation in transcriptional upregulation and H3K27me3 depletion was not clearly evident (Figure 5H). However, there were other HSCidentity genes upregulated in *Jarid2*-KO^{Vav} HSCs and MPPs, such as *Grb10* and *Hoxb5*, that were not associated with H3K27me3 changes (Figure S5G). These data demonstrate that JARID2 is responsible for epigenetic repression of self-renewal genetic programs in committed hematopoietic progenitors by recruiting PRC2 to gene bodies to establish H3K27me3.

Mycn and Runx1t1 Co-expression Endows MPPs with Self-Renewal Potential

As Runx1t1 and Mycn can help reprogram committed blood cells to a multipotent state (Riddell et al., 2014), we tested if overexpression of Runx1t1 and Mycn individually or together in wild-type MPPs would phenocopy loss of *Jarid2*. BM progenitors were transduced with lentiviruses expressing Runx1t1, Mycn or Runx1t1-T2A-Mycn and transplanted into recipient mice. 12 weeks post-transplant, 100 donor-derived GFP^{+} MPPs were purified from BM and transplanted into secondary recipients with 2.5×10^5 WBM competitor cells. Mycn and Runx1t1 co-expression in wild-type MPPs endowed long-term multi-lineage repopulating capacity *in vivo* (Figure 6A,B). 91% (10/11) of mice transplanted with Runx1t1 and Mycn co-expressing MPPs were classified as LTMR (Figure 6C). Co-

expression of both Runx1t1 and Mycn was required for a fully-penetrant phenotype (Figure 6C). BM analysis revealed that only MPPs coexpressing Runx1t1 and Mycn underwent robust self-renewal (Figure 6D,E). Co-expression of Runx1t1 and Mycn in MPPs induced expression of HSC fingerprint genes analogous to deletion of *Jarid2* (Figure S6A). Runx1t1 and Mycn over-expression was sustained for the duration of the transplant (Figure S6B). On the other hand, over-expressing Runx1t1 and Mycn in wild-type HSCs did not affect differentiation (Figure S6C), as 100% (5/5) of mice transplanted with Runx1t1/Mycn-expressing HSCs were LTMR (Figure S6D). This suggests that the context of Runx1t1 and Mycn as JARID2 target genes is more important in MPPs, although co-expression of Runx1t1 and Mycn in wild-type HSCs did amplify self-renewal in the BM (Figure S6E).

We next aimed to ameliorate self-renewal in *Jarid2*-KO MPPs by knock-down of Runx1t1 and/or Mycn. BM progenitors from *Jarid2*-KO^{Vav} mice were transduced with shRNA-expressing lentiviruses (Figure 6F) and transplanted. As MPPs are the major cell population in *Jarid2*KO^{Vav} BM with robust engraftment potential, the long-term hematopoietic output from the transduced cell fraction largely reflects activity of MPPs. Initial transduction efficiencies were comparable (Figure 6G). shRNA targeting Mycn alone or together with Runx1t1 exhibited significantly reduced peripheral blood contribution compared to cells expressing the LacZtargeting negative control shRNA (Figure 6H). Knock-down of Runx1t1 alone in *Jarid2*-KO^{Vav} MPPs did not have any effect on peripheral blood chimerism (Figure 6I), despite the fact that Runx1t1 was more effectively inhibited by the shRNA than Mycn in *Jarid2*-KO^{Vav} MPPs (Figure S6F). This suggests that *Mycn* is more important than *Runx1t1* for conveying self-renewal potential to *Jarid2*-KO^{Vav} MPPs.

JARID2 Regulates Overlapping Mechanisms in Normal and Malignant Hematopoiesis

As the most frequent MPN mutation preceding *JARID2* deletion is *JAK2*^{V617F} (Milosevic et al., 2012; Puda et al., 2012), a mouse model of inducible *Jak2*^{V617F} mutation that develops MPN (Mullally et al., 2010) was crossed to Mx1-CRE:*Jarid2*$^{fl/fl}$ mice. In Mx1-CRE:*Jarid2*fl/+*Jak2*V617F/+ (*Jarid2*-HETMx1:*Jak2*V617F) and Mx1-CRE:*Jarid2*fl/fl*Jak2*V617F/+ (*Jarid2*KO^{Mx1}:*Jak2*^{V617F}) mice, activation of *Jak2*^{V617F} and deletion of *Jarid2* occur simultaneously in the BM upon injection of pIpC. Deletion of *Jarid2* in a *Jak2*^{V617F} background in eight week old mice accelerated the development of MPN with a median survival of 19 and 42 days for *Jarid2*KO^{Mx1}:*Jak2*^{V617F} and *Jarid2*-HET^{Mx1}:*Jak2*^{V617F} mice respectively, compared to 104 days for *Jak2*^{V617F} mice (Figure 7A). Accelerated mortality in *Jarid2*-mutant mice was attributed to increased thrombosis, particularly splanchnic vein thrombosis (Figure 7B), a common condition in young female *JAK2*^{V617F}–positive MPN patients (How et al., 2017). Deficiency for *Jarid2* enhanced MPN pathologies such as leukocytosis, neutrophilia, polycythemia, thrombocytosis (Figure 7C), BM hypercellularity and splenomegaly (Figure S7A). Although we did not observe BM fibrosis, pockets of reticulin fibers were evident in the spleens of *Jarid2*-HET^{Mx1}*Jak2*^{V617F} and *Jarid2*-KO^{Mx1}*Jak2*^{V617F} mice, and much more prevalent than in *Jak2*^{V617F} mice (Figure 7D). There was increased megakaryopoiesis in the BM of *Jarid2*-KO^{Mx1}*Jak2*^{V617F} mice, and in the spleens of the red pulp was expanded, with extensive extramedullary hematopoiesis and effacement of splenic architecture (Figure 7D). Leukemic transformation in

*Jarid2*KO^{Mx1}:*Jak2*^{V617F} mice was not observed, possibly because they succumbed to thrombotic complications before sAML could develop.

Like in normal hematopoiesis, HSCs and MPPs were also depleted in *Jarid2*KO^{Mx1}:*Jak2*^{V617F} mice (Figure S7B). Studies show that *Jak2*^{V617F} HSCs are responsible for initiation of MPN (Lundberg et al., 2014; Mullally et al., 2012). To determine if inactivation of *Jarid2* altered the MPN-initiating cell population, 500 HSCs and MPPs were isolated from *Jak2*^{V617F} and *Jarid2*-KO^{Mx1}:*Jak2*^{V617F} mice two weeks post-pIpC and transplanted into sublethally irradiated mice. Blood analysis showed that *Jarid2*-KO^{Mx1}:*Jak2*^{V617F} MPPs can engraft and propagate disease (Figure S7C). MPN pathologies mediated by *Jarid2*KO^{Mx1}:*Jak2*^{V617F} MPPs was comparable to that of *Jak2*^{V617F} HSCs (Figure S7C). *Jarid2*KO^{Mx1}:*Jak2*^{V617F} HSCs were unable to produce peripheral blood, possibly because complete loss of *Jarid2* renders them unable to escape quiescence or overcome differentiation block. Mirroring the function of JARID2 in normal hematopoietic development, these data suggest the identity of MPN-initiating cells shifts from HSCs to MPPs when *Jarid2* is deleted in a *Jak2*^{V617F} mutant background. However, we cannot rule out that *Jarid2*-KO^{Mx1}:*Jak2*^{V617F} HSCs could still contain MPN-initiating potential under different physiological stresses (or non-transplant conditions).

RNA-seq was performed on HSCs and MPPs from Control^{Mx1}, *Jak2*^{V617F} and *Jarid2*KO^{Mx1}:*Jak2*^{V617F} mice two weeks post-pIpC treatment (Table S2). GSEA revealed that the top downregulated gene set in *Jarid2*-KO^{Mx1}:*Jak2*^{V617F} HSCs was G_2/M checkpoint genes (Figure S7D), again suggesting these HSCs remain trapped in quiescence. *Jarid2*-KO^{Mx1}:*Jak2*^{V617F} HSCs and MPPs showed upregulation of *Hoxa* cluster genes (Figure S7E), a well-described pathogenic mechanism in AML (Bach et al., 2010; Spencer et al., 2015). Because the phenotype of *Jarid2*-KO^{Mx1}:*Jak2*^{V617F} mice differed from that of *Ezh2*-KO:*Jak2*^{V617F} mice, we compared gene expression signatures from our study to that of *Ezh2*-KO:*Jak2*^{V617F} HSCs (Shimizu et al., 2016). Although *Jak2*^{V617F} mice deficient for *Ezh2* also show accelerated MPN with fibrosis (Shimizu et al., 2016; Yang et al., 2016), the latency of disease onset is much longer than our model. There was no overlap in the genes downregulated in *Jarid2*KO^{Mx1}:*Jak2*^{V617F} HSCs and *Ezh2*-KO:*Jak2*^{V617F} HSCs compared to *Jak2*^{V617F} HSCs, but 79 genes (Table S3) in common that were upregulated from the same comparisons (Figure S7F). Thus, both phenotypically and mechanistically (Figure S7G), the functions of Ezh2 and Jarid2 are not entirely overlapping and Jarid2 may have non-canonical (PRC2-independent) functions as a hematopoietic tumor suppressor. The latter explanation is supported by co-immunoprecipitation in mouse thymocytes showing that while almost all Jarid2 appears to be associated with PRC2, only a fraction of PRC2 is bound by Jarid2 (Figure S5A).

Further analysis revealed that of the gene sets significantly upregulated in *Jarid2*KO^{Mx1}:*Jak2*^{V617F} HSCs, 5/11 (45%) were involved in cytokine signaling (Figure 7E). Although JAK/STAT signaling is elevated in *Jak2*^{V617F} HSCs, this pathway was even more active in *Jarid2*KO^{Mx1}:*Jak2*^{V617F} progenitor cells (Figure 7F), and myeloid cells from *Jarid2*-KO^{Mx1}:*Jak2*^{V617F} mice were hypersensitive to IL-6 (Figure 7F). The mechanism for this cytokine hypersensitivity may include the 30-fold upregulation of *Mpl* in *Jarid2*-KO^{Mx1}:*Jak2*^{V617F} HSCs (Figure S7H). *Jarid2* expression was sharply induced after acute

induction of *Jak2*^{V617F} mutation in HSCs, an effect not observed in response to other common MPN- and MDS-initiating mutations (Figure 7G). *Jarid2* may function as a tumor suppressor in response to *Jak2*^{V617F} mutations by restraining JAK/STAT signaling.

Inhibition of JARID2 in MPN Patient-Derived Cells

To determine if JARID2 had similar functions in human hematopoiesis, HEL cells (human *JAK2*^{V617F}-mutant erythroleukemia line) with *JARID2* knockout were created. Many murine mechanisms were conserved in *JARID2*-null HEL cells, including increased phosphorylated STAT3, and upregulation of Runx1t1, Mycn and Hoxa9 (Figure S8A). Analysis of gene expression data (Norfo et al., 2014), revealed that *JARID2* is downregulated in the majority of myelofibrosis (MF) (Figure S8B), but not polycythemia vera (PV; (Spivak et al., 2014)) or essential thrombocythemia (ET; (Puigdecanet et al., 2008)) patient samples (Figure S8C). In MF, *JARID2* downregulation was accompanied by *MYCN* upregulation, but no change in *RUNX1T1* expression (Figure S8B). Flow cytometric analysis (Figure S8D) revealed that HSCs and MPPs were increased in MF compared to normal BM (Figure S8E). Lentiviral shRNAs targeting JARID2 were generated (Figure 8A) and CD34^{+} cells from MF patients (Table S4) were transduced with two independent JARID2 shRNAs (in parallel with shLacZ negative control). 48-hours post-transduction, 500 Lineage^{-}CD38^{-}CD34^{+}GFP^{+} (transduced) cells were purified and assayed for colony-forming potential. Across five independent cases, inhibition of JARID2 consistently yielded higher colony-forming potential, both in terms of total numbers and after normalization to control for variability between individual cases (Figure 8B). This suggested that like in mice, inhibition of JARID2 may increase self-renewal of human hematopoietic progenitors.

As human MF cells are refractory to growth in patient-derived xenograft (PDX) models, we hypothesize that JARID2 inhibition may allow these cells to engraft immunodeficient mice. CD34^{+} cells from MF patients were transduced with lentiviral shRNAs, then transplanted into sublethally irradiated NOD-scid *Il2rg*-null-3/GM/SF (NSGS) mice via X-ray guided intra-tibial injection. JARID2 inhibition facilitated long-term peripheral blood engraftment, which was only transient in control LacZ transduced cells (Figure 8C). Analysis 12 weeks post-transplant (Figure 8D) identified robust BM engraftment from MF cells with decreased JARID2 (Figure 8E). Inhibition of JARID2 produced other hallmarks of MPN such as splenomegaly (Figure S8F), polycythemia, thrombocytosis (Figure S8G) and amyeloid maturational arrest (left shift) in the BM (Figure S8H). Sequencing confirmed the *JAK2*^{V617F} mutation was still present in the engrafted cells (Figure S8I). JARID2 inhibition induced marked reticulin fibrosis in the BM (Figure 8F).

Because *Runx1t1* and *Mycn* were also upregulated in *Jarid2*-KO^{Mx1}:*Jak2*^{V617F} progenitors (Figure S7G), we asked if over-expressing them in MF cells would also phenocopy inhibition of JARID2. Ectopic expression of human Runx1t1 and/or Mycn in MF cells increased colonyforming potential (Figure S8J). In PDX models, ectopic expression of Runx1t1 and Mycn did not produce peripheral blood engraftment. But 12 weeks post-transplant, Runx1t1/Mycn overexpressing cells were readily detectable in the BM (Figure S8K) and were able to transmit reticulin fibrosis (Figure S8L). Thus, *RUNX1T1* and *MYCN* are key target genes of JARID2 in human progenitors and over-expression of them is able to

recapitulate some of the properties of JARID2 inhibition, but other JARID2 target genes are required to fully manifest the phenotype.

DISCUSSION

The molecular mechanisms by which repression of self-renewal potential occurs in committed hematopoietic progenitors is largely unknown. We found that inactivation of *Jarid2* removed constraints limiting self-renewal in MPPs. JARID2`s ability to silence self-renewal networks in progenitor cells reveals a mechanism by which deletions of this gene may contribute to oncogenesis. Acceleration of MPN and transformation to sAML could be due to acquisition of self-renewal potential in a cell population carrying a driver mutation that normally lacks this capacity. The epigenetic landscape or proliferative capacity of MPPs may provide a more permissive context for leukemic transformation compared to HSCs. Acquisition of selfrenewal potential in committed progenitor cells is an oncogenic mechanism in other systems such as MLL-AF9-driven AML (Krivtsov et al., 2013).

Although loss of *Jarid2* co-operated with *Jak2*^{V617F} mutation, there was no evidence of transformation to sAML. Post-MPN sAML was only obtained from genetic deletion of *Jarid2* in a pre-existing neoplastic background (driven by IDH2^{R140Q}), as is the case in patients, demonstrating the impact of order of mutation acquisition on disease biology. The pathogenic cooperation between *Jak2*^{V617F} and *Jarid2* deletion suggests JARID2 has specific tumor suppressor functions in response to *Jak2*^{V617F} mutation. JARID2 was acutely induced in HSCs immediately upon acquiring *Jak2*^{V617F} mutation, and loss of *Jarid2* in a *Jak2*^{V617F} mutant background further amplified JAK/STAT signaling. Our data suggests the tumor suppressor function of JARID2 in response to *Jak2*^{V617F} mutations relates to its ability to restrain JAK/STAT signaling and prevent the malignant clone from acquiring the necessary self-renewal properties required for transformation to sAML. Interestingly, JARID2 expression was similarly induced in HSCs following *Flt3*^{ITD} mutation, which also activates STAT signaling (Choudhary et al., 2007).

Two downstream targets of JARID2, *Runx1t1* and *Mycn*, are at least partially responsible for endowing long-term multi-lineage potential to *Jarid2*-KO MPPs. These genes were also upregulated in *Jarid2*-KO^{Mx1}:*Jak2*^{V617F} MPN, presenting the possibility that inhibition of Runx1t1 and Mycn could be exploited as a therapeutic strategy in sAML. Analysis of H3K27me3 profiles showed that JARID2 recruits PRC2 to gene bodies to facilitate epigenetic repression of self-renewal networks in hematopoietic progenitor cells. However, several upregulated HSCidentity genes in *Jarid2*-KO^{Vav} MPPs were not associated with changes in repressive chromatin. These may be indirect consequences of *Jarid2* inactivation, or perhaps be repressed by PRC2independent functions of JARID2. Clearly, recruitment of PRC2 by JARID2 is of critical importance for regulation of hematopoietic progenitors, but perhaps not all activities of JARID2 are PRC2-dependent.

While other PDX models have reported engraftment of human MPN cells (James et al., 2008; Reinisch et al., 2016), inhibition of JARID2 in primary MF cells permitted engraftment and transmission of reticulin fibrosis in our PDX system. Osteopetrotic trabecular bone formation was a feature of both mouse and human transplant models of

JARID2-deificent progenitor cells, suggesting non-cell autonomous signals resulting from JARID2 inhibition contribute to pathologies in the BM.

In summary, our findings demonstrate that JARID2 represses self-renewal networks in MPPs as a mechanism to restrict long-term repopulating capacity to the most primitive HSCs. We demonstrate that JARID2 is a hematopoietic tumor suppressor, and open the possibility for therapeutic strategies in patients with *JARID2*-deleted hematopoietic malignancies. The observation that *JARID2* is repressed in a large fraction of MF cases suggests our findings may be more broadly applicable to a wide range of these patients regardless of genetic background. Moreover, it is possible the frequency of chromosomal deletions encompassing *JARID2* in postMDS/MPN sAML are under-represented as targeted genome sequencing approaches become more prevalent.

STAR METHODS

CONTACT FOR REAGENT AND RESOURCE SHARING

Further information and requests for resources and reagents should be directed to and will be fulfilled by the Lead Contact, Grant Challen (gchallen@dom.wustl.edu).

EXPERIMENTAL MODEL AND SUBJECT DETAILS

Animals—All animal procedures were approved by the Institutional Animal Care and Use Committee of Washington University. All mice used in this study were C57Bl/6 background. *Jarid2*$^{fl/fl}$ mice were obtained from Dr. Youngsook Lee (University of Wisconsin). *Jak2*^{V617F} mice were obtained from Dr. Ann Mullally (Brigham and Women's Hospital). CRE-dependent *Rosa26*$^{Cas9\text{-}GFP}$ mice were obtained from The Jackson Laboratory (#026175). In these mice, the Cas9 transgene is driven by a CAG promoter downstream of a loxP-STOP-loxP cassette to render Cas9 and GFP expression inducible by CRE recombinase (Platt et al., 2014). Mice carrying floxed alleles were crossed to either Mx1-CRE or Vav-CRE strains. For strains carrying Mx1-CRE, recombination of floxed alleles was induced by intraperitoneal injection of six doses (300 μg / mouse) of polyinosinic–polycytidylic acid (pIpC; Sigma #P1350) given every other day. 10–12 weeks old mice were typically used for experimentation. Equal numbers of male and female mice were used, no gender biases were noted. 8 weeks old male and female mice C57Bl/6 CD45.1 mice (The Jackson laboratory) were used as recipients for bone marrow transplantation assays.

Human MPN Samples—Peripheral blood or bone marrow samples were obtained with written consent according to a protocol approved by the Washington University Human Studies Committee (WU no. 011014) in accordance with the Declaration of Helsinki protocol. De-identified mononuclear cells (PB or BM mononuclear cells) were obtained by Ficoll gradient extraction from cryopreserved specimens according to standard procedures. Clinical and genetic information for patients studied is included in Table S3. Genomic data for these patients has been previously described (Fisher et al., 2017). $CD34^{+}$ cells were isolated from individual patients by flow cytometry for experimentation.

Cell Lines—HEL 92.1.7 (ATCC TIB-180) cells were grown in complete RPMI 1640 medium (ATCC #30–2001) supplemented with 10% FBS and 100 units/mL Pen-Strep at 37ºC and 5% CO_2. 32D cells (ATCC CRL-11346) were grown in RPMI 1640 medium (Gibco #11875–085) supplemented with 10% FBS, 100 units/mL Pen-Strep and 5 ng/mL mouse IL-3 at 37ºC and 5% CO_2. 293T cells (ATCC CRL-3216) were grown in Dulbecco's Modified Eagle's Medium (Gibco #11965084) supplemented with 10% FBS, 2 nM L-glutamine, and 100 units/mL Pen-Strep at 37ºC and 5% CO_2.

METHOD DETAILS

Bone Marrow Transplantation—C57Bl/6 CD45.1 recipient mice were transplanted by retro-orbital injection after a split dose (~4-hours apart) of 10.5 Gy of lethal irradiation, or a single dose of 6.0 Gy for sublethal irradiation in tumor studies. For competitive transplants, a standardized number of phenotypically-defined hematopoietic stem cells (HSCs), multipotent progenitors (MPPs), restricted progenitors (RPs), or whole bone marrow (WBM) were transplanted into lethally irradiated recipients along with 2.5×10^5 wild-type CD45.1 WBM. In transplanted recipients, donor cells can be distinguished from wild-type competitor cells via CD45 allelic isoforms, with CD45.2 discriminating donor-derived cells and CD45.1 marking competitor-derived (and matched to the recipient). For serial HSC and MPP transplantation, 100 donor-derived HSCs ($CD45.2^+Lineage^-c\text{-}Kit^+Sca\text{-}1^+CD48^-CD150^+$) or MPPs ($CD45.2^+Lineage^-c\text{-}Kit^+Sca\text{-}1^+CD48CD150^-$) were isolated from primary recipients 18 weeks post-transplant by FACS and transplanted into lethally irradiated recipients along with freshly isolated 2.5×10^5 wild-type WBM competitor. Transplanted recipients were bled every four-weeks and analyzed for donor-derived lineage contribution in peripheral blood by flow cytometry using the following cell surface markers: $Gr\text{-}1^+$ and $Mac\text{-}1^+$ (myeloid lineage), $B220^+$ (B cell lineage), $CD3e^+$ (T cell lineage), as well as CD45.2 and CD45.1 to discriminate donor- versus competitor-derived peripheral blood contribution. For limiting dilution transplants, either 2×10^4, 5×10^4 or 1×10^5 WBM cells from either $Control^{Vav}$ or *Jarid2*-KO^{Vav} mice were transplanted into lethally irradiated recipients along with 2.5×10^5 wild-type CD45.1 WBM by retro-orbital injection. Transplanted recipients were bled every four-weeks and analyzed as above. Recipients with greater than 1% donor-derived chimerism to myeloid, B cell and T cell blood lineages at 16 weeks post-transplant were considered long-term multi-lineage reconstitution (LTMR). For xenotransplantations, $CD34^+$ hematopoietic stem and progenitor cells isolated were isolated from *JAK2*^{V617F}-positive MF patients by flow cytometry. Sorted $CD34^+$ cells were incubated in Stempro-34 medium (Gibco #10639011) supplemented with Pen-Strep (100 Units/mL), L-glutamine (2 mM), human stem cell factor (SCF; 50 ng/mL), human thrombopoietin (TPO; 150 ng/mL), human Flt3L (50 ng/mL) and human interleukin-6 (IL-6; 50 ng/mL). 12–24 hr post-sort, cells were transduced with highhigh titer lentiviruses and were transplanted into sublethally irradiated (200 rads) NOD-scid*Il2rg*-null-3/GM/SF (NSGS; The Jacksons Laboratory #013062) mice via X-ray guided intra-tibial injections. Engraftment of human cells in xenotransplants were assessed by flow cytometry with an antibody against human CD45. Table S3 includes detailed information for patient samples as well as number of transduced cells used to transplant into NSGS recipients in this study.

Cell Purification and Flow Cytometry Overview—WBM was isolated from femurs, tibias and iliac crests. All antibody staining was performed in HBSS buffer (Corning #21021CV) containing Pen/Strep (100 Units/mL; Fisher Scientific #MT30002CI), HEPES (10uM; Life Technologies # 15630080) and FBS (2%; Sigma #14009C). Briefly, cells were suspended in complete HBSS at a concentration of 5×10^8 cells/mL and incubated on ice for 20 min with the desired antibodies listed in Key Resources Table. For cell sorting, magnetic enrichment was carried out using the AutoMACS Pro Seperator (Miltenyi Biotec) with mouse CD117-conjugated microbeads (Miltenyi Biotec #130–091-224). Postenrichment, the positive cell fraction was stained with appropriate antibodies and sorted by FACS. Side population staining on WBM was performed with Hoechst 33342 (Sigma #B2261) as previously described (Goodell et al., 1996). All antibodies utilized in this study were used at 1:100 dilutions and were obtained from BioLegend, eBioscience or BD Biosciences unless otherwise stated.

Plasmids and Viral Transduction—Mouse Mycn and Runx1t1 cDNAs were kindly provided by Dr. Derrick Rossi (Harvard Stem Cell Institute). Wild-type mouse IDH2 cDNA was obtained from Transomic (#BC060030). The R140Q mutation was introduced using the site-directed mutagenesis kit according to manufacturer's instructions (Agilent Technologies #200522–5). $IDH2^{R140Q}$, Runx1t1 and Mycn cDNA were PCR amplified using primer pairs IDH2_Forw_AscI // IDH2_Rev_XhoI, Runx1t1_Forw_AscI // Runx1t1_Rev_SphI, Mycn_Forw_AscI // Mycn_Rev_HpaI (Key Resources Table), respectively and cloned into the HIV-pMND-IRES-GFP lentiviral vector as previously described (Schuettpelz et al., 2012). For cloning of Runx1t1 and Mycn in a polycistronic fashion, Runx1t1 and Mycn coding sequences were PCR amplified using following primer pairs: Runx1t1_Forw_AscI // Runx1t1_Rev_SphI, Mycn_Forw_AscI // Mycn_Rev_HpaI and sequentially cloned into HIV-pMND-IRES-GFP lentiviral vector to yield HIV-pMND-Runx1t1. Mycn-IRES-GFP, which is further digested using Sbf1 and BstBI restriction enzymes, in which a gene block that carry 3'end of Runx1t1, a T2A coding sequence and 5'sequence of Mycn is cloned. The final vector is called pMND-Runx1t1-T2A-Mycn-IRES-GFP.

For lentiviral production, 293T cells were co-transfected with the packaging plasmids pMD.G, psPAX2 and either with empty pMND-IRES-GFP, pMND-$IDH2R^{140Q}$-IRES-GFP, pMNDRunx1t1-IRES-GFP, pMND-Mycn-IRES-GFP, pMND-Runx1t1-T2A-Mycn-IRES-GFP, Lenti_gRNA_LacZ_EFS_BFP, Lenti_gRNA_m*Jarid2*#1_EFS_BFP or Lenti_sgRNA_m*Jarid2*#2_EFS_BFP using PEI-based transfection protocol (Polysciences cat# 23966–1). Transfections for lentiviral production were performed in 150×25 mm tissue culture dishes (Falcon #353025) when 293T cells reached >80% confluency. 48 hr post-transfection, 293T cell supernatants were collected and concentrated by centrifugation at 76,000 g for 1.5 hr at 4°C. For lentiviral transduction, c-Kit $^+$ BM cells were isolated using magnetic enrichment and adjusted to 5×10^5 cells/100 μL in Stempro-34 medium (Gibco #10639011) supplemented with Pen-Strep (100 Units/mL), L-glutamine (2 mM), murine stem cell factor (100 ng/mL), murine thrombopoietin (100 ng/mL), murine Flt3L (50 ng/mL), murine interleukin-3 (5 ng/mL), polybrene (4 μg/mL; Sigma), and spin-infected with lentivirus preparations at 250 g for 2 hr in 96 well plate format. 24 hr post-transduction, 1×10^5

transduced cells were transplanted into lethally irradiated mice (following a split dose of 10.5 Gy of irradiation) by retro-orbital injection.

For retroviral production, 293T cells were co-transfected with the packaging plasmid pCL-ECO and either with *Jak2*^{V617F}, *IDH2*^{R140Q}, *Mpl*^{S15L}, *Kras*^{G12D}, and *Flt3*^{ITD} in the MSCV-IRESGFP (MIG) as previously described. 48 hr post-transfection, 293T cell supernatants were collected and concentrated by Retro-X concentrator (Clontech, #631455).

Multipotent progenitor cell (MPP) transplants from *Rosa26*$^{Cas9\text{-}GFP}$ mice—Cas9 expressing MPPs (GFP$^+$Lineage$^-$c-Kit$^+$Sca-1$^+$CD48$^-$CD150$^-$) were isolated from 10 weeks Vav-CRE:*Rosa26*$^{Cas9\text{-}GFP/+}$ mice (Platt et al., 2014) by flow cytometry and transduced with Lenti_gRNA_EFS_BFP expressing gRNA targeting exon 3 of *Jarid2* (gRNA#1 – [5’ ->3]’: ATTTTGAAGAAGGGCCGTCG, gRNA#2 – [5’ ->3]’: GCTAGTAGAGGACACTTGGG) or Exon 1 of *Ezh2* (gRNA#1 – [5’ ->3]’: ACACCACCTAAACGCCCAGG, gRNA#2 – [5’ ->3]’: CAAGGGCACGAACTGTCACA). The experiment also included a non-targeting negative control gRNA ([5’ ->3]’: GCGAGGTATTCGGCTCCGCG). 48 hr post-transduction, 200 transduced cells (GFP$^+$BFP$^+$Lineage$^-$c-Kit$^+$Sca-1$^+$CD48$^-$CD150$^-$) were transplanted into lethally irradiated recipients along with 2.0 ×10^5 wild-type CD45.1 WBM by retro-orbital injection. Transplanted recipients were bled every four-weeks and analyzed as previously described.

***in vivo* shRNA-based knock-down—**c-Kit+ BM cells from 10 weeks old *Jarid2*-KO^{Vav} mice were transduced with combination of pLKO.1-GFP or pLKO.1-mCherry expressing shRNAs targeting Runx1t1 and/or Mycn. c-Kit+ cells were split into four equal groups for transduction with each of the following viral cocktails: LacZ1_pLKO.1-GFP // shLacZ2_pLKO.1-mCherry, shLacZ1_pLKO.1-mCherry // shRunx1t1_pLKO.1-GFP, shLacZ1_pLKO.1-mCherry // shMycn_pLKO.1-GFP, shRunx1t1_pLKO.1-mCherry // shMycn_pLKO.1-GFP. All shRNAs are expressed in pLKO.1 plasmid lentivirus with the following target sequences (5’ -> 3’): LacZ#1: ACTCTGGCTAACGGTACGCGT, LacZ#2 CCGTCATAGCGATAACGAGTT, Mycn#1: GATACCTTGAGCGACTCAGAT, Runx1t1#1: GCAAGCTGAAACGATTTCTTA. CD34$^+$ cells isolated from *JAK2*^{V617F}-positive MF patients were transduced with pLKO.1-GFP expressing shRNA targeting JARID2 (target sequence: GAAACAGGTTTCTAAGGTAAA) in parallel with LacZ negative control shRNA (target sequence: GAAACAGGTTTCTAAGGTAAA).

Colony forming assays—For human Methocult studies, 500 CD34$^+$CD38$^-$Lineage$^-$ cells expressing shRNAs targeting JARID2 or overexpressing RUNX1T1-T2A-MYCN were sorted by flow cytometry directly into Methocult M3045 medium (Stem Cell Technologies #04035). Two weeks post-sort, colonies were scored under inverted microscope (Nikon eclipse TS100). Two independent shRNAs that effectively silence the expression of JARID2 (in parallel with LacZ negative control shRNAs) were used for this study.

For mouse Methocult studies, 150 MPPs from Control^{Vav} or *Jarid2*-KO^{Vav} mice were sorted directly into Methocult M3434 medium (Stem Cell Technologies #03434) and cultured *in vitro* at 37°C. Colony-forming units (CFUs) were scored after seven days, then cells were

collected, pooled, and re-plated at a density of 10,000 cells per well for a total of three successive plates.

Methocult-based HSC genotyping—Floxing efficiency was checked by sorting single HSCs from either *Jarid2*-KO^{Vav} or *Jarid2*-KO^{Mx1} mice into 96-well plates containing Methocult M3434 medium (Stem Cell Technologies #03434) and grown for two weeks. Individual colonies were collected and washed with Dulbecco's Phosphate Buffered Saline (Sigma #D8537), and genomic DNA was isolated using the KAPA Express Extract Kit (Sigma # KK7103). To confirm the deletion of Exon 3, we performed PCR using primer pairs: Jarid2-FloxO-F//Jarid2-FloxO-R (Mysliwiec et al., 2006).

Quantitative Real-Time PCR—Total RNA was isolated using the Nucleospin RNA XS (Macherey-Nagel #740902–250) and reverse transcribed with the SuperScript VILO kit (Invitrogen #11754–050). cDNA input was standardized and real-time PCR was performed with Taqman master Mix (Applied Biosystems #4304437), 18 s-rRNA probe (VIC-MGB; Applied Biosystems #74319413E), and a gene-specific probe (FAM-MGB; Applied Biosystems (Key Resources Table)) on a StepOnePlus RealTime PCR System (Life Technologies). Samples were normalized to 18S and fold-change determined by the ¨¨Ct method.

Ki67 and Annexin V staining—WBM was stained with cell surface markers as described. For intracellular Ki67/7AAD (cell cycle) staining, cells were fixed and permeabilized using Cytofix/Cytoperm kit according to manufacturer's protocol (BD #554714) and stained with an anti-Ki67-BV605 (BioLegend #652413) for 1 hr at room temperature. 7AAD (BioLegend #420404) was added to samples and allowed to incubate for 20 min before analysis by flow cytometry. For AnnexinV apoptosis assay, WBM was washed twice with cold PBS and incubated at room temperature for 15 min in 1× binding buffer (10 mM HEPES, 140 mM NaCl and 2.5 mM $CaCl_2$) containing AnnexinV– APC (eBiScience #88–8007-72) and 7AAD. Cells were analyzed by flow cytometry within 1 hr of staining.

5-FU survival assay—5-Fluorouracil (5-FU; Sigma-Aldrich F6627) was administered intraperitoneally into mice previously transplanted with 5×10^5 WBM from Control^{Vav} or *Jarid2*-KO^{Vav} mice along with 5×10^5 wild-type CD45.1 WBM cells. 5-FU was administered at weekly intervals (150 mg/kg) until mice became moribund.

BrdU incorporation—5×10^5 WBM cells isolated from either Control^{Vav} or *Jarid2*-KO^{Vav} was transplanted into lethally irradiated recipients along with 5×10^5 wild-type CD45.1 WBM by retro-orbital injection. Eight weeks post-transplant, a single dose of 5-FU (150 mg/kg; Sigma-Aldrich F6627–1G) was injected at the same time as BrdU (3.33mg/mouse; Sigma #B5002) via intra-peritoneal route, and BrdU (0.8mg/mL) was supplemented in the drinking water for 96 hr prior to harvest. For unmanipulated mice, two doses of 5-FU (150 mg/kg) were injected seven days apart, with BrdU (3.33mg/mouse) injected via intra-peritoneal route at the same time as the second 5-FU injection, and BrdU (0.8mg/mL) was supplemented in the drinking water for 96 hr prior to harvest. For BrdU analysis, 10×10^6 WBM cells were stained with cell surface markers overnight at 4^{o}C followed by staining

with anti-BrdU-APC (BD Pharmingen #51–9000019AK) according to the manufacturer's directions.

Cytospins and Histopathology—For cytospins, 1×10^6 cells were collected in 100μL PBS/2% FBS from single cell preparations of BM, added to Shandon Single Cytofunnels (Thermo Scientific #1102548) clipped to glass slides (FisherScientific #12–550-20), and centrifuged using a Cytospin 3 centrifuge (Shandon) set at 500 rpm for 5 min at medium acceleration. After drying, cells were stained with the Hema 3 stat pack (Fisher Scientific #23–123869) and images captured with a Nikon Eclipse E200 microscope equipped with an Infinity 2 color camera (Lumenera) controlled by Infinity Capture software (Lumenera).

For histopathology, mouse tibia and spleens were fixed in 10% neutral buffered formalin (Fisher Scientific #SF100–4) overnight at 4ºC or 1 hr at room temperature, respectively. Spleens were inoculated in 35% sucrose (Fisher Scientific #525590A) overnight, whereas bones were decalcified (Calrite from Richard-allen Scientific #5501) for 12 days prior to overnight inoculation in 35% sucrose. Both tibias and spleens were rinsed with PBS and processed for paraffin embedding and sectioned at 5 μM. Both H&E and reticulin staining was performed by the Histology Lab of Washington University. Images were captured using an inverted microscope and analyzed with NIS-Elements software from Nikon.

Co-Immunoprecipitation and Western Blot—Co-Immunoprecipitation was performed using 500 μg of thymus tissue lysate. Briefly, 3 μg of sheep polyclonal JARID2 antibody (R&D systems #AF6090) or 3 μg of rabbit polyclonal Suz12 (Abcam #ab12073) immumo-precipitated overnight with 8 μl of Dynabeads Protein G (Invitrogen #10003D). Polyclonal Sheep (Abcam, #ab37385) or Rabbit polyclonal IgG (Milipore, #12–370) isotype controls used to exclude the possibility of unspecific interactions. Washing steps were performed according to manufacturer's protocol. Elutions were performed in 6×SDS reducing buffer. For western blot, 10–20 μg of protein samples were separated in pre-casted 415% gradient SDS gels (Biorad #456–1084) and transferred to nitrocellulose membranes (Millipore #IPVH00010). Membranes were subsequently probed to detect proteins using primary antibodies listed in Key Resources Table and detection was performed using horseradishperoxidase conjugated secondary mouse, rabbit or sheep antibody and chemiluminescence HRP substrate (Millipore #WBKLS0100). For co-immunoprecipitated protein detection, VeriBlot IP Detection Reagent (Abcam, #ab131366) was used to avoid interference from denatured IgG.

For the detection of pSTAT3 in BM myeloid cells, 4.0×10^6 $Gr1^+Mac1^+$ cells were sorted by flow cytometry and incubated in RPMI base medium (Gibco, #11875–085) containing IL6 (5ng/mL; Miltenyi Biotec, #130–096-682) for 30 min at 37ºC. Western blot was then performed as mentioned previously.

RNA-sequencing—Total RNA was extracted using the NucleoSpin RNA XS kit (Macherey-Nagel #740902) from purified HSCs and MPPs as biological replicates from pooled $Control^{Vav}$ and *Jarid2*-KO^{Vav} mice (equal numbers males and females), or from $Control^{Mx1}$, *Jak2*^{V617F} and *Jak2*^{V617F}:*Jarid2*KO^{Mx1} mice. Library preparation was performed with 3–5 ng of total RNA using the SMARTer Ultra Low RNA kit (Clontech) and

sequenced on an Illumina HiSeq-3000. RNA-seq reads were aligned to the Ensembl release 76 top-level assembly with STAR version 2.0.4b. Gene counts were derived from the number of uniquely aligned unambiguous reads by Subread:featureCount version 1.4.5. Transcript counts were produced by Sailfish version 0.6.3. Sequencing performance was assessed for total number of aligned reads, total number of uniquely aligned reads, genes and transcripts detected, ribosomal fraction known junction saturation and read distribution over known gene models with RSeQC version 2.3. All gene-level and transcript counts were then imported into the R/Bioconductor package EdgeR and TMM normalization size factors were calculated to adjust for samples for differences in library size. Genes or transcripts not expressed in any sample were excluded from further analysis. The TMM size factors and the matrix of counts were then imported into R/Bioconductor package Limma and weighted likelihoods based on the observed meanvariance relationship of every gene/transcript were then calculated for all samples with the Voom function. Performance of the samples was assessed with a spearman correlation matrix and multi-dimensional scaling plots.

Gene/transcript performance was assessed with plots of residual standard deviation of every gene to their average log-count with a robustly fitted trend line of the residuals. Generalized linear models were then created to test for gene/transcript level differential expression. Differentially expressed genes and transcripts were then filtered for unadjusted $p<0.05$. Primary RNA-seq data is available under GEO accession number GSE120595.

ChIP-mentation—ChIP-mentation was conducted as described previously (Schmidl et al., 2015). 1×10^4 HSCs and MPPs were sorted into PBS with 10% FBS. Cells were crosslinked with 1% paraformaldehyde at room temperature for 8 min. Chromatin was sheared with an E220 Focused-ultrasonicator (Covaris) until the majority of DNA fragments were between 200 and 700 bp, and subsequently incubated with H3K27me3 antibody (Diagenode # pAb-069–050) overnight at 4°C. Protein G dynabeads (Life Technologies # 130–099-508) were added to the chromatin/antibody incubation for an additional 2 hr at 4°C. Following washes, the beads were tagmented for 10 min at 37°C.The beads underwent additional washes before the immunoprecipitated DNA was isolated by decrosslinking and purified with Ampure XP beads (Beckman Coulter #NC9959336). DNA library amplification was performed using 2×Kapa HiFi HotStart Ready Mix (Kapa #KB KK2601), Nextera custom primers, and 12 cycles of PCR as determined by qPCR. Libraries were purified with Ampure XP beads and run on an Illumina Hiseq 3000 (PE2X150). Sequences were aligned to mm10 using Bowtie2. Peak calling of H3K27me3 was performed with hiddenDomains and quality metrics assessed with the R package, ChIPQC. Regions of differential H3K27me3 (>1.7 fold difference) with a corrected (Benjamini/Hochberg) $p<0.01$ were determined using THOR from the Regulatory Genomics Toolbox suite of programs.Differential H3K27me3 regions were annotated using HOMER. Heatmaps depicting variable H3K27me3 in and around gene bodies were constructed using deepTools. Primary Chip-mentation data is available under GEO accession number GSE120595.

CRISPR/Cas9 mediated gene knock out—Using the web interface of UCSC Genome Browser's CRISPR design software (https://genome.ucsc.edu/), multiple small guide RNAs (gRNAs) targeting either exon 1 of mouse *Jarid2* or *Ezh2* genes, or exon 3 of mouse or

human *Jarid2*/*JARID2* genes were designed. Off-target activity of these gRNAs were further evaluated with Blastn (https://blast.ncbi.nlm.nih.gov/Blast.cgi). Two complementary oligos were designed to generate double stranded gRNA with flanking BsmBI restriction sites. The sequences of the gRNAs used in this study are listed in Key Resources Table. These oligos were self-annealed and cloned into BsmBI digested LRB plasmid (Lenti_sgRNA_EFS_BFP). This is a modified version of Lenti_sgRNA_EFS_GFP (Addgene #65656), where GFP was replaced by blue fluorescent protein (BFP). 32D or HEL cells stably expressing Cas9 in which the expression of Cas9 is linked to GFP via an internal ribosome entry site (IRES) were transduced with lentiviruses to express either mouse or human gRNAs, respectively. 48 hr post-transduction, stable cell lines expressing both Cas9 and gRNA were established by sorting GFP^+BFP^+ cells by FACS. Upon expansion of these cells, western blot was performed to validate successful inactivation of the target gene.

QUANTIFICATION AND STATISTICAL ANALYSIS

Student t-test and ANOVA's were used for statistical comparisons where appropriate. Survival curves were analyzed by Mantel–Cox logrank test. Significance is indicated using the following convention: *p<0.05, **p<0.01, ***p<0.001, ****p<0.0001. Error bars on graphs represent the standard error of the mean (S.E.M.).

DATA AND SOFTWARE AVAILABILITY

Primary RNA-seq and ChIP-mentation data is available under GEO accession number GSE120595.

Supplementary Material

Refer to Web version on PubMed Central for supplementary material.

ACKNOWLEDGEMENTS

The authors declare no conflicts of interest. *Jak2*^{V617F} mice were from Dr. Ann Mullally (Brigham and Women's Hospital). Mycn and Runx1t1 cDNAs were from Dr. Derrick Rossi (Harvard Stem Cell Institute). We thank the Siteman Flow Cytometry Core, supported by CA91842, and the Genome Technology Access Center, supported by CA91842 and UL1TR000448. This work was supported by the American Society of Hematology, the V Foundation, the Sidney Kimmel Foundation and Gabrielle's Angel Foundation. HC was supported by the American Society of Hematology and the EvansMDS Foundation. WCW was supported by NIH T32HL008088. CM was supported by NIH T32HL008088, and NIH F31DK111058–01. ELO was supported by NIH 5T32CA113275–10 and NIH F31DK114951. GAC is a Leukemia and Lymphoma Society scholar.

REFERENCES

Abdulkarim K, Girodon F, Johansson P, Maynadie M, Kutti J, Carli PM, Bovet E, and Andreasson B (2009). AML transformation in 56 patients with Ph- MPD in two well defined populations. Eur J Haematol 82, 106–111. [PubMed: 19134023]

Bach C, Buhl S, Mueller D, Garcia-Cuellar MP, Maethner E, and Slany RK (2010). Leukemogenic transformation by HOXA cluster genes. Blood 115, 2910–2918. [PubMed: 20130239]

Cancer Genome Atlas Research, Ley N, Miller TJ, Ding CL, Raphael BJ, Mungall AJ, Robertson A, Hoadley K, Triche TJ, Jr., Laird PW, et al. (2013). Genomic and epigenomic landscapes of adult de novo acute myeloid leukemia. N Engl J Med 368, 20592074.

Cao R, Wang L, Wang H, Xia L, Erdjument-Bromage H, Tempst P, Jones RS, and Zhang Y (2002). Role of histone H3 lysine 27 methylation in Polycomb-group silencing. Science 298, 1039–1043. [PubMed: 12351676]

Cervantes F, Tassies D, Salgado C, Rovira M, Pereira A, and Rozman C (1991). Acute transformation in nonleukemic chronic myeloproliferative disorders: actuarial probability and main characteristics in a series of 218 patients. Acta Haematol 85, 124–127. [PubMed: 2042444]

Challen GA, Sun D, Mayle A, Jeong M, Luo M, Rodriguez B, Mallaney C, Celik H, Yang L, Xia Z, et al. (2014). Dnmt3a and Dnmt3b Have Overlapping and Distinct Functions in Hematopoietic Stem Cells. Cell Stem Cell.

Chambers SM, Boles NC, Lin KY, Tierney MP, Bowman TV, Bradfute SB, Chen AJ, Merchant AA, Sirin O, Weksberg DC, et al. (2007). Hematopoietic fingerprints: an expression database of stem cells and their progeny. Cell Stem Cell 1, 578–591. [PubMed: 18371395]

Chen JY, Miyanishi M, Wang SK, Yamazaki S, Sinha R, Kao KS, Seita J, Sahoo D, Nakauchi H, and Weissman IL (2016). Hoxb5 marks long-term haematopoietic stem cells and reveals a homogenous perivascular niche. Nature 530, 223–227. [PubMed: 26863982]

Choudhary C, Brandts C, Schwable J, Tickenbrock L, Sargin B, Ueker A, Bohmer FD, Berdel WE, Muller-Tidow C, and Serve H (2007). Activation mechanisms of STAT5 by oncogenic Flt3-ITD. Blood 110, 370–374. [PubMed: 17356133]

Fisher DAC, Malkova O, Engle EK, Miner CA, Fulbright MC, Behbehani GK, Collins TB, Bandyopadhyay S, Zhou A, Nolan GP, and Oh ST (2017). Mass cytometry analysis reveals hyperactive NF Kappa B signaling in myelofibrosis and secondary acute myeloid leukemia. Leukemia 31, 1962–1974. [PubMed: 28008177]

Gazit R, Mandal PK, Ebina W, Ben-Zvi A, Nombela-Arrieta C, Silberstein LE, and Rossi DJ (2014). Fgd5 identifies hematopoietic stem cells in the murine bone marrow. J Exp Med 211, 1315–1331. [PubMed: 24958848]

Georgiades P, Ogilvy S, Duval H, Licence DR, Charnock-Jones DS, Smith SK, and Print CG (2002). VavCre transgenic mice: a tool for mutagenesis in hematopoietic and endothelial lineages. Genesis 34, 251–256. [PubMed: 12434335]

Goodell MA, Brose K, Paradis G, Conner AS, and Mulligan RC (1996). Isolation and functional properties of murine hematopoietic stem cells that are replicating in vivo. J Exp Med 183, 1797–1806. [PubMed: 8666936]

How J, Zhou A, and Oh ST (2017). Splanchnic vein thrombosis in myeloproliferative neoplasms: pathophysiology and molecular mechanisms of disease. Ther Adv Hematol 8, 107118.

James C, Mazurier F, Dupont S, Chaligne R, Lamrissi-Garcia I, Tulliez M, Lippert E, Mahon FX, Pasquet JM, Etienne G, et al. (2008). The hematopoietic stem cell compartment of JAK2V617F-positive myeloproliferative disorders is a reflection of disease heterogeneity. Blood 112, 2429–2438. [PubMed: 18612101]

Jeong M, Park HJ, Celik H, Ostrander EL, Reyes JM, Guzman A, Rodriguez B, Lei Y, Lee Y, Ding L, et al. (2018). Loss of Dnmt3a Immortalizes Hematopoietic Stem Cells In Vivo. Cell Rep 23, 1–10. [PubMed: 29617651]

Kogan SC, Ward JM, Anver MR, Berman JJ, Brayton C, Cardiff RD, Carter JS, de Coronado S, Downing JR, Fredrickson TN, et al. (2002). Bethesda proposals for classification of nonlymphoid hematopoietic neoplasms in mice. Blood 100, 238–245. [PubMed: 12070033]

Krivtsov AV, Figueroa ME, Sinha AU, Stubbs MC, Feng Z, Valk PJ, Delwel R, Dohner K, Bullinger L, Kung AL, et al. (2013). Cell of origin determines clinically relevant subtypes of MLL-rearranged AML. Leukemia 27, 852–860. [PubMed: 23235717]

Kuhn R, Schwenk F, Aguet M, and Rajewsky K (1995). Inducible Gene Targeting in Mice. Science 269, 1427–1429. [PubMed: 7660125]

Lee SC, Miller S, Hyland C, Kauppi M, Lebois M, Di Rago L, Metcalf D, Kinkel SA, Josefsson EC, Blewitt ME, et al. (2015). Polycomb repressive complex 2 component Suz12 is required for hematopoietic stem cell function and lymphopoiesis. Blood 126, 167–175. [PubMed: 26036803]

Lu C, Han HD, Mangala LS, Ali-Fehmi R, Newton CS, Ozbun L, Armaiz-Pena GN, Hu W, Stone RL, Munkarah A, et al. (2010). Regulation of tumor angiogenesis by EZH2. Cancer Cell 18, 185–197. [PubMed: 20708159]

Lundberg P, Takizawa H, Kubovcakova L, Guo G, Hao-Shen H, Dirnhofer S, Orkin SH, Manz MG, and Skoda RC (2014). Myeloproliferative neoplasms can be initiated from a single hematopoietic stem cell expressing JAK2-V617F. J Exp Med 211, 2213–2230. [PubMed: 25288396]

Mesa RA, Li CY, Ketterling RP, Schroeder GS, Knudson RA, and Tefferi A (2005). Leukemic transformation in myelofibrosis with myeloid metaplasia: a single-institution experience with 91 cases. Blood 105, 973–977. [PubMed: 15388582]

Milosevic JD, Puda A, Malcovati L, Berg T, Hofbauer M, Stukalov A, Klampfl T, Harutyunyan AS, Gisslinger H, Gisslinger B, et al. (2012). Clinical significance of genetic aberrations in secondary acute myeloid leukemia. Am J Hematol 87, 1010–1016. [PubMed: 22887079]

Mochizuki-Kashio M, Mishima Y, Miyagi S, Negishi M, Saraya A, Konuma T, Shinga J, Koseki H, and Iwama A (2011). Dependency on the polycomb gene Ezh2 distinguishes fetal from adult hematopoietic stem cells. Blood 118, 6553–6561. [PubMed: 22042701]

Mullally A, Lane SW, Ball B, Megerdichian C, Okabe R, Al-Shahrour F, Paktinat M, Haydu JE, Housman E, Lord AM, et al. (2010). Physiological Jak2V617F expression causes a lethal myeloproliferative neoplasm with differential effects on hematopoietic stem and progenitor cells. Cancer Cell 17, 584–596. [PubMed: 20541703]

Mullally A, Poveromo L, Schneider RK, Al-Shahrour F, Lane SW, and Ebert BL (2012). Distinct roles for long-term hematopoietic stem cells and erythroid precursor cells in a murine model of Jak2V617F-mediated polycythemia vera. Blood 120, 166–172. [PubMed: 22627765]

Mysliwiec MR, Chen J, Powers PA, Bartley CR, Schneider MD, and Lee Y (2006). Generation of a conditional null allele of jumonji. Genesis 44, 407–411. [PubMed: 16900512]

Norfo R, Zini R, Pennucci V, Bianchi E, Salati S, Guglielmelli P, Bogani C, Fanelli T, Mannarelli C, Rosti V, et al. (2014). miRNA-mRNA integrative analysis in primary myelofibrosis CD34+ cells: role of miR-155/JARID2 axis in abnormal megakaryopoiesis. Blood 124, e21–32. [PubMed: 25097177]

Passamonti F, Rumi E, Arcaini L, Castagnola C, Lunghi M, Bernasconi P, Giovanni Della Porta M, Columbo N, Pascutto C, Cazzola M, and Lazzarino M (2005). Leukemic transformation of polycythemia vera: a single center study of 23 patients. Cancer 104, 10321036.

Platt RJ, Chen S, Zhou Y, Yim MJ, Swiech L, Kempton HR, Dahlman JE, Parnas O, Eisenhaure TM, Jovanovic M, et al. (2014). CRISPR-Cas9 knockin mice for genome editing and cancer modeling. Cell 159, 440–455. [PubMed: 25263330]

Puda A, Milosevic JD, Berg T, Klampfl T, Harutyunyan AS, Gisslinger B, Rumi E, Pietra D, Malcovati L, Elena C, et al. (2012). Frequent deletions of JARID2 in leukemic transformation of chronic myeloid malignancies. Am J Hematol 87, 245–250. [PubMed: 22190018]

Puigdecanet E, Espinet B, Lozano JJ, Sumoy L, Bellosillo B, Arenillas L, AlvarezLarran A, Sole F, Serrano S, Besses C, and Florensa L (2008). Gene expression profiling distinguishes JAK2V617F-negative from JAK2V617F-positive patients in essential thrombocythemia. Leukemia 22, 1368–1376. [PubMed: 18480837]

Rampal R, Ahn J, Abdel-Wahab O, Nahas M, Wang K, Lipson D, Otto GA, Yelensky R, Hricik T, McKenney AS, et al. (2014). Genomic and functional analysis of leukemic transformation of myeloproliferative neoplasms. Proc Natl Acad Sci U S A 111, E5401–5410. [PubMed: 25516983]

Reinisch A, Thomas D, Corces MR, Zhang X, Gratzinger D, Hong WJ, Schallmoser K, Strunk D, and Majeti R (2016). A humanized bone marrow ossicle xenotransplantation model enables improved engraftment of healthy and leukemic human hematopoietic cells. Nat Med 22, 812–821. [PubMed: 27213817]

Riddell J, Gazit R, Garrison BS, Guo G, Saadatpour A, Mandal PK, Ebina W, Volchkov P, Yuan GC, Orkin SH, and Rossi DJ (2014). Reprogramming committed murine blood cells to induced hematopoietic stem cells with defined factors. Cell 157, 549–564. [PubMed: 24766805]

Schmidl C, Rendeiro AF, Sheffield NC, and Bock C (2015). ChIPmentation: fast, robust, low-input ChIP-seq for histones and transcription factors. Nat Methods 12, 963–965. [PubMed: 26280331]

Schuettpelz LG, Gopalan PK, Giuste FO, Romine MP, van Os R, and Link DC (2012). Kruppel-like factor 7 overexpression suppresses hematopoietic stem and progenitor cell function. Blood 120, 2981–2989. [PubMed: 22936656]

Shimizu T, Kubovcakova L, Nienhold R, Zmajkovic J, Meyer SC, Hao-Shen H, Geier F, Dirnhofer S, Guglielmelli P, Vannucchi AM, et al. (2016). Loss of Ezh2 synergizes with JAK2-V617F in initiating myeloproliferative neoplasms and promoting myelofibrosis. J Exp Med 213, 1479–1496. [PubMed: 27401344]

Spencer DH, Young MA, Lamprecht TL, Helton NM, Fulton R, O'Laughlin M, Fronick C, Magrini V, Demeter RT, Miller CA, et al. (2015). Epigenomic analysis of the HOX gene loci reveals mechanisms that may control canonical expression patterns in AML and normal hematopoietic cells. Leukemia 29, 1279–1289. [PubMed: 25600023]

Spivak JL, Considine M, Williams DM, Talbot CC, Jr., Rogers O, Moliterno AR, Jie C, and Ochs MF (2014). Two clinical phenotypes in polycythemia vera. N Engl J Med 371, 808–817. [PubMed: 25162887]

Tallarico M, and Odenike O (2015). Secondary acute myeloid leukemias arising from Philadelphia chromosome negative myeloproliferative neoplasms: pathogenesis, risk factors, and therapeutic strategies. Curr Hematol Malig Rep 10, 112–117. [PubMed: 25893311]

Walter MJ, Shen D, Ding L, Shao J, Koboldt DC, Chen K, Larson DE, McLellan MD, Dooling D, Abbott R, et al. (2012). Clonal architecture of secondary acute myeloid leukemia. N Engl J Med 366, 1090–1098. [PubMed: 22417201]

Xie H, Xu J, Hsu JH, Nguyen M, Fujiwara Y, Peng C, and Orkin SH (2014). Polycomb repressive complex 2 regulates normal hematopoietic stem cell function in a developmental-stage-specific manner. Cell Stem Cell 14, 68–80. [PubMed: 24239285]

Yang Y, Akada H, Nath D, Hutchison RE, and Mohi G (2016). Loss of Ezh2 cooperates with Jak2V617F in the development of myelofibrosis in a mouse model of myeloproliferative neoplasm. Blood 127, 3410–3423. [PubMed: 27081096]

HIGHLIGHTS

- JARID2 is a *bona fide* tumor suppressor in chronic myeloid neoplasms.
- JARID2 restricts self-renewal in multipotent hematopoietic progenitors.
- Mycn and Runx1t1 co-expression provides wild-type MPPs with HSC-like potential.
- JARID2 inhibition transmits myelofibrosis in patient-derived xenografts.

JARID2 is recurrently deleted in acute myeloid leukemia progressed fron myeloproliferative neoplasms ans myelodsplastic syndromes. Celik et al.show that JARID2 recruits PRC2 to repress the expression of self-renewal networks, of which Mycn and Runx1t1 are important factors, in hematopoietic progenitor cells.

SIGNIFICANCE

Post-MPN/MDS sAML is a devastating disease with dismal clinical outcomes. Greater understanding of the contribution of specific genetics events in leukemic transformation of chronic myeloid diseases is required for the development of targeted therapies. This study showed that in combination with prototypical driver mutations, deletion of *Jarid2* either accelerated development of MPN or drove transformation to sAML, depending on the timing and context of mutational acquisition. Mechanistically, JARID2 recruits PRC2 to gene bodies to epigenetically repress expression of self-renewal networks in hematopoietic progenitor cells. Loss of *Jarid2* conveyed self-renewal to multipotent progenitor cells, driven by de-repression of *Runx1t1* and *Mycn*. JARID2 inhibition facilitated engraftment of patient-derived myelofibrosis cells in immunodeficient mice and transmitted pathologies including reticulin fibrosis.

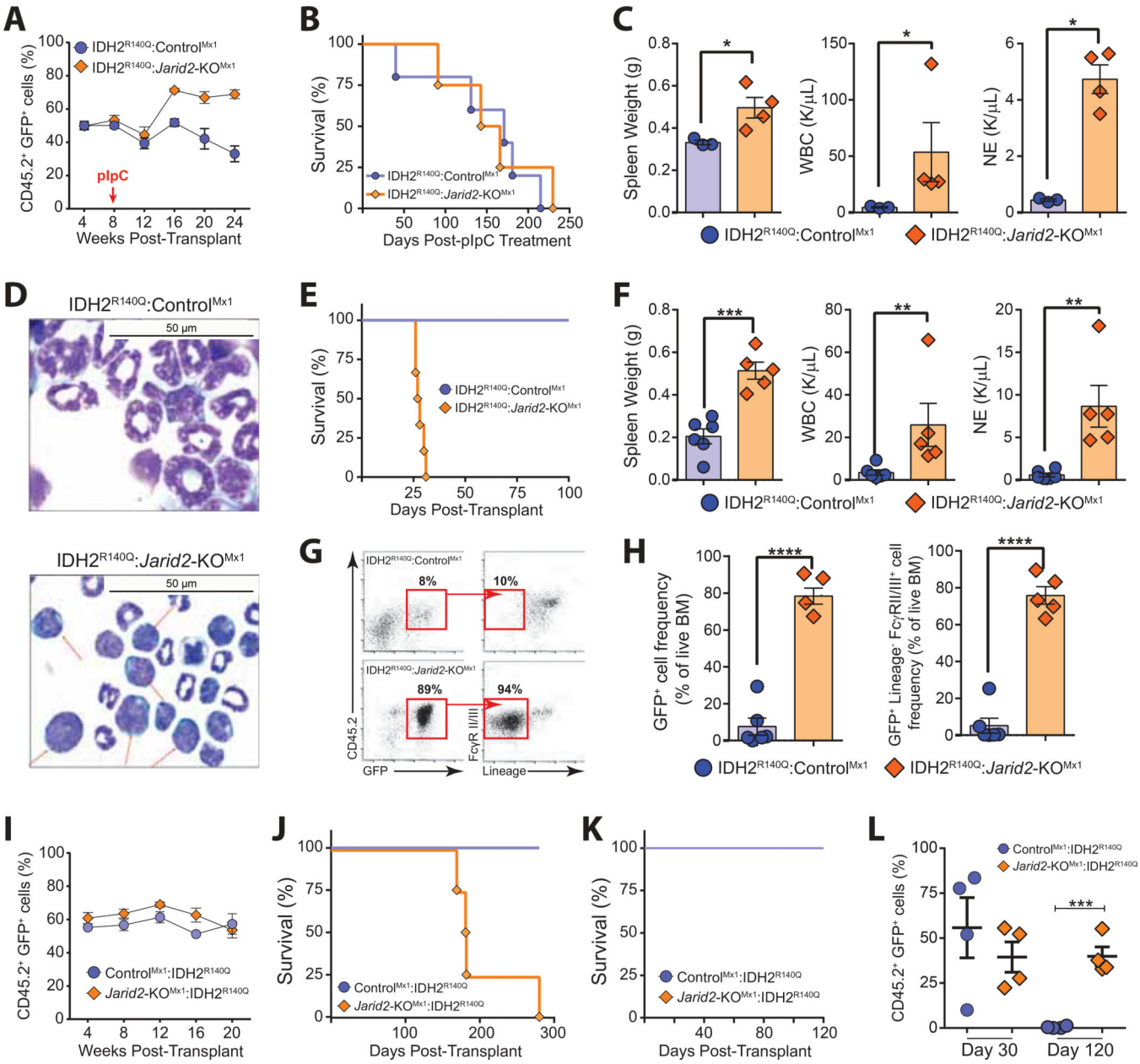

Figure 1: JARID2 is a Hematopoietic Tumor Suppressor.

(A) Percent of donor-derived IDH2^{R140Q}-expressing cells in peripheral blood of recipient mice. Deletion of *Jarid2* was induced eight weeks post-transplant (n=4–5).

(B) Kaplan-Meier plot comparing survival of mice transplanted with IDH2^{R140Q}:Control^{Mx1} or IDH2^{R140Q}:*Jarid2*-KO^{Mx1} cells (n=4–5).

(C) Spleen weights and blood counts of moribund mice (n=3–4).

(D) Bone marrow cytospins of moribund mice. Red arrows indicate AML blasts.

(E) Kaplan-Meier plot comparing survival of secondary recipients transplanted with BM from moribund primary mice (n=6).

(F) Spleen weights and blood counts of secondary recipients (n=5–6).

(G) Representative flow cytometry plots of secondary recipient mice showing AML blasts ($CD45.2^{+}GFP^{+}Lineage^{-}FcgRII/III^{+}$).

(H) Frequency of donor-derived GFP^{+} cells (left) and donor-derived AML blasts (right) in the BM of secondary recipients (n=5–6).

(I) Percent of donor-derived $IDH2^{R140Q}$-expressing cells in blood of recipient mice. Deletion of *Jarid2* was induced eight weeks prior to $IDH2^{R140Q}$ transduction and transplantation (n=4).

(J) Kaplan-Meier plot comparing survival of recipient mice transplanted with $Control^{Mx1}$:$IDH2^{R140Q}$ or *Jarid2*-KO^{Mx1}:$IDH2^{R140Q}$ cells (n=4). *Jarid2* was deleted prior to introduction of $IDH2^{R140Q}$.

(K) Kaplan-Meier plot comparing survival of secondary recipients transplanted with BM from primary $Control^{Mx1}$:$IDH2^{R140Q}$ and *Jarid2*-KO^{Mx1}:$IDH2^{R140Q}$ mice (n=4).

(L) Percent of donor-derived $IDH2^{R140Q}$-expressing cells in the blood of secondary $Control^{Mx1}$:$IDH2^{R140Q}$ and *Jarid2*-KO^{Mx1}:$IDH2^{R140Q}$ recipient mice.

In F – H, $IDH2^{R140Q}$:*Jarid2*-KO^{Mx1} values are from moribund mice at time of sacrifice, whereas $IDH2^{R140Q}$:$Control^{M1}$ values are taken from mice at day 100 post-transplant. *p<0.05, **p<0.01, ***p<0.001, ****p<0.0001. Mean ± S.E.M. values are shown. See also Figure S1.

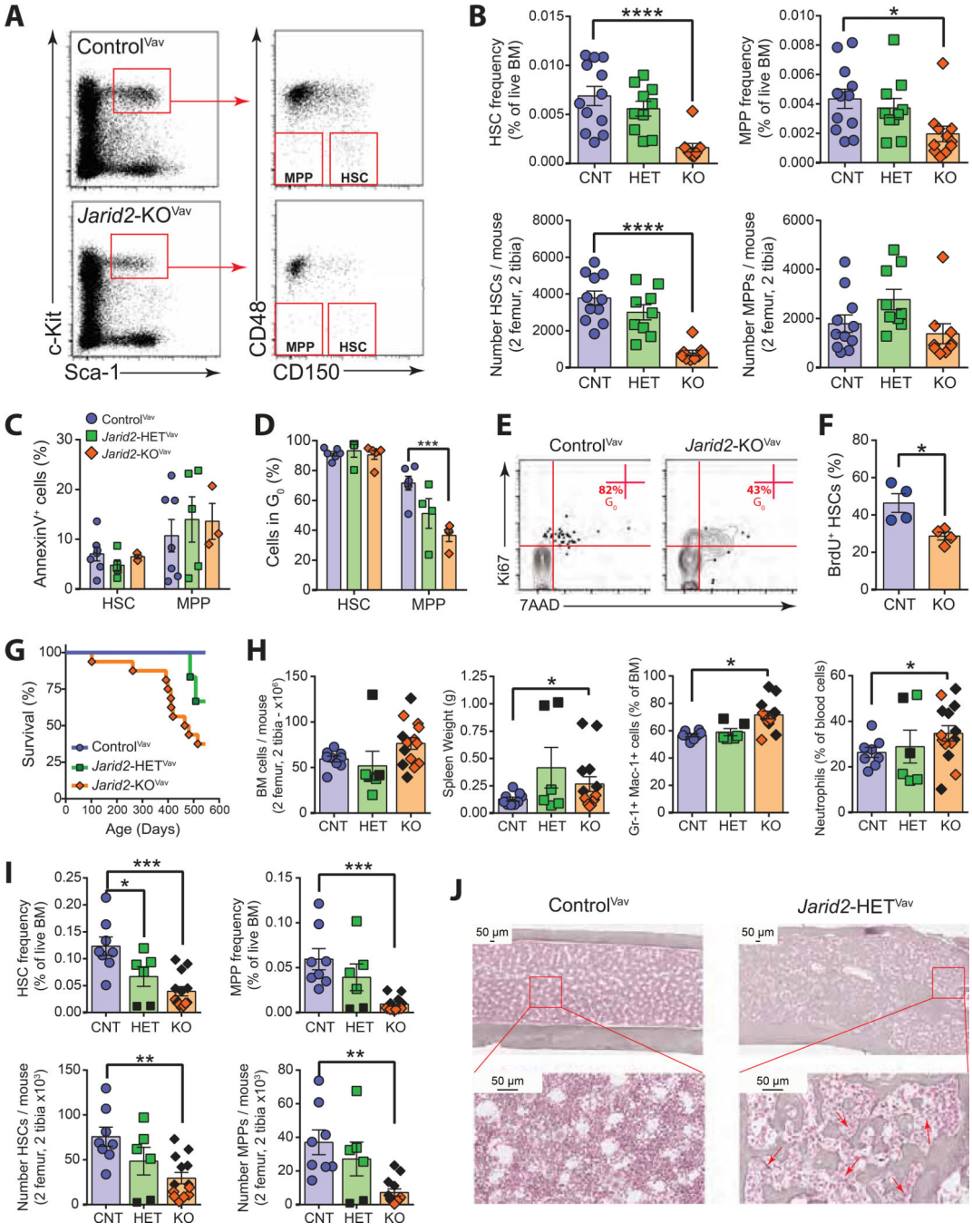

Figure 2: Loss of JARID2 Leads to Depletion of Primitive Hematopoietic Progenitors.

(A) Flow cytometry plots showing definition of HSCs and MPPs in BM of ten weeks old mice.

(B) Quantification of HSCs and MPPs in BM of ten weeks old Control^{Vav} (CNT, n=12), *Jarid2*-HET^{Vav} (HET, n=10) and *Jarid2*-KO^{Vav} (KO, n=10) mice.

(C) Frequency of apoptotic (AnnexinV^{+}) HSCs and MPPs in ten weeks old mice (n=3–6).

(D) Frequency of quiescent (G_0) HSCs and MPPs in ten weeks old mice (n=3–6).

(E) Representative flow cytometry plots showing cell cycle analysis of MPPs.

(F) Quantification of 96 hr BrdU incorporation in HSCs following two doses of 5-FU.
(G) Kaplan-Meier plot comparing survival between Control^{Vav} (n=10), *Jarid2*-HET^{Vav} (n=10), and *Jarid2*-KO^{Vav} (n=16) mice.
(H) Pathological analysis showing BM hypercellularity, splenomegaly, and increased myeloid cells in the BM and blood of moribund *Jarid2*-HET^{Vav} and *Jarid2*-KO^{Vav} mice.
(I) Quantification of HSCs and MPPs in BM of moribund mice.
(J) Bone histology section showing trabecular bone formation and reticulin fibrosis (red arrows).
In H and I, colored shapes represent quantifications taken from non-moribund mice at day 550, whereas black-filled shapes are from moribund mice at time of sacrifice. Control^{Vav} mice were sacrificed at day 550 for analysis. *p<0.05, **p<0.01, ***p<0.001, ****p<0.0001. Mean ± S.E.M. values are shown. See also Figure S2.

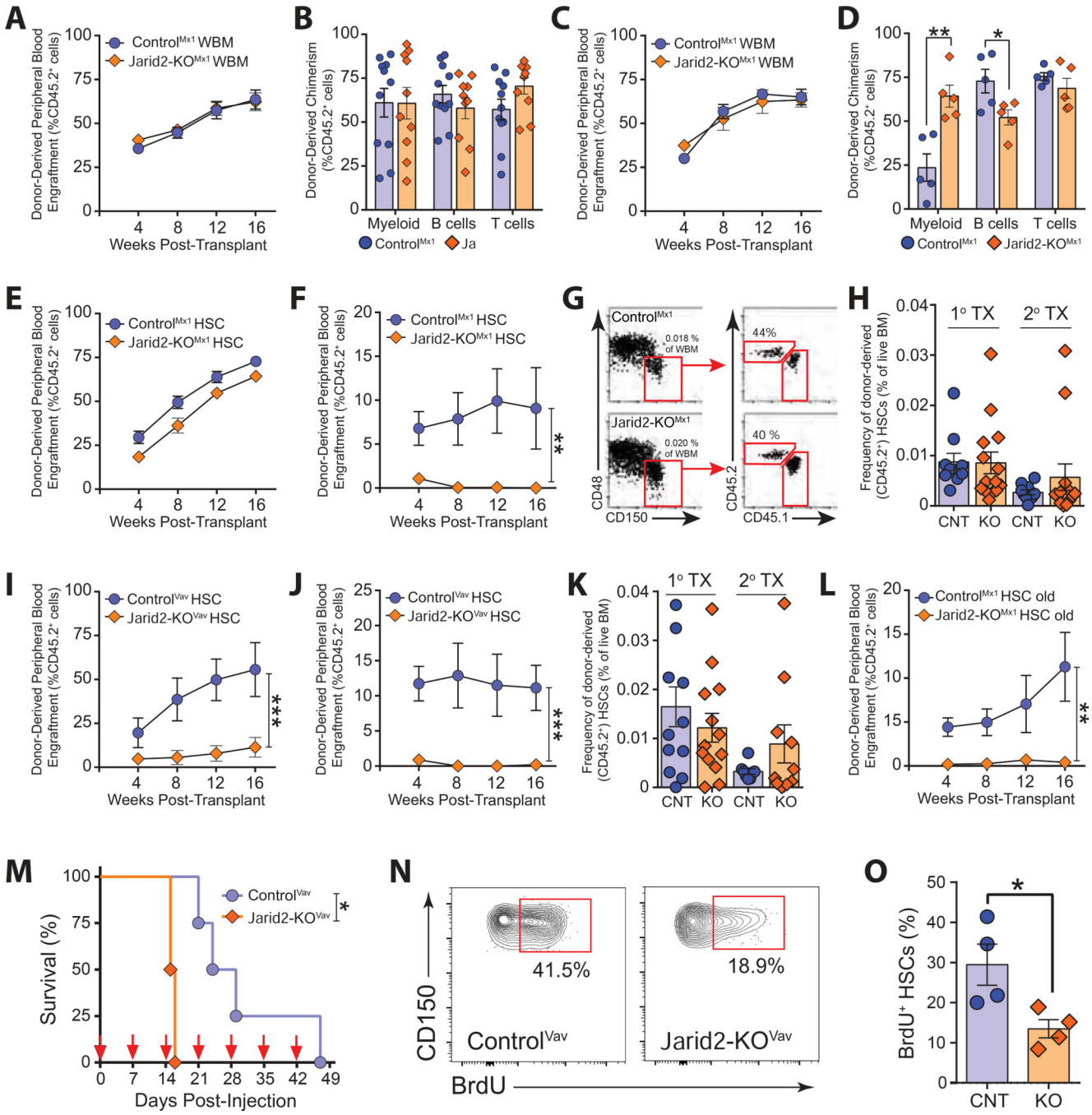

Figure 3: HSCs Lacking JARID2 Have Defective Differentiation.

(A) Contribution of Control^{Mx1} (n=11) and *Jarid2*-KO^{Mx1} (n=10) WBM to primary recipient peripheral blood.

(B) Chimerism of donor-derived WBM cells in myeloid, B and T cell lineages in primary recipients at 16 weeks post-transplant.

(C) Contribution of Control^{Mx1} (n=5) and *Jarid2*-KO^{Mx1} (n=5) WBM to secondary recipient peripheral blood.

(D) Chimerism of donor-derived WBM cells in myeloid, B and T cell lineages in secondary recipients at 16 weeks post-transplant.
(E) Contribution of 100 purified Control^{Mx1} (n=11) or *Jarid2*-KO^{Mx1} (n=14) HSCs to primary recipient peripheral blood.
(F) Contribution of 100 purified Control^{Mx1} (n=6) or *Jarid2*-KO^{Mx1} (n=5) HSCs to secondary recipient peripheral blood.
(G) Representative flow cytometry plots showing donor-derived HSCs in the BM of recipient mice at 18 weeks post-secondary transplant.
(H) Frequency of donor-defined HSCs (CD45.2^{+}Lineage^{-}c-Kit^{+}Sca-1^{+}CD48^{-}CD150^{+}) in the BM of recipients transplanted with Control^{Mx1} or *Jarid2*-KO^{Mx1} HSCs at 18 weeks posttransplant.
(I) Contribution of 100 purified Control^{Vav} (n=4) or *Jarid2*-KO^{Vav} (n=5) HSCs to primary recipient peripheral blood.
(J) Contribution of 100 purified Control^{Vav} (n=8) or *Jarid2*-KO^{Vav} (n=7) HSCs to secondary recipient peripheral blood.
(K) Frequency of donor-defined HSCs in the BM of recipients transplanted with Control^{Vav} or *Jarid2*-KO^{Vav} HSCs at 18 weeks post-transplant.
(L) Contribution of 100 purified Control^{Mx1} (n=4) or *Jarid2*-KO^{Mx1} (n=4) HSCs from mice 12 months post-pIpC to primary recipient peripheral blood.
(M) Kaplan-Meier plot comparing survival between mice with chimeric Control^{Vav} (n=4) and *Jarid2*-KO^{Vav} (n=4) BM given weekly injections of 5-FU (red arrows).
(N) Flow cytometry gating showing BrdU analysis of HSCs from mice with chimeric BM treated with 5-FU.
(O) Quantification of 96 hr BrdU incorporation in HSCs from mice with Control^{Vav} (CNT, n=4) and *Jarid2*-KO^{Vav} (KO, n=4) chimeric BM following a single dose of 5-FU.
*p<0.05, **p<0.01, ***p<0.001. Mean ± S.E.M. values are shown. See also Figure S3.

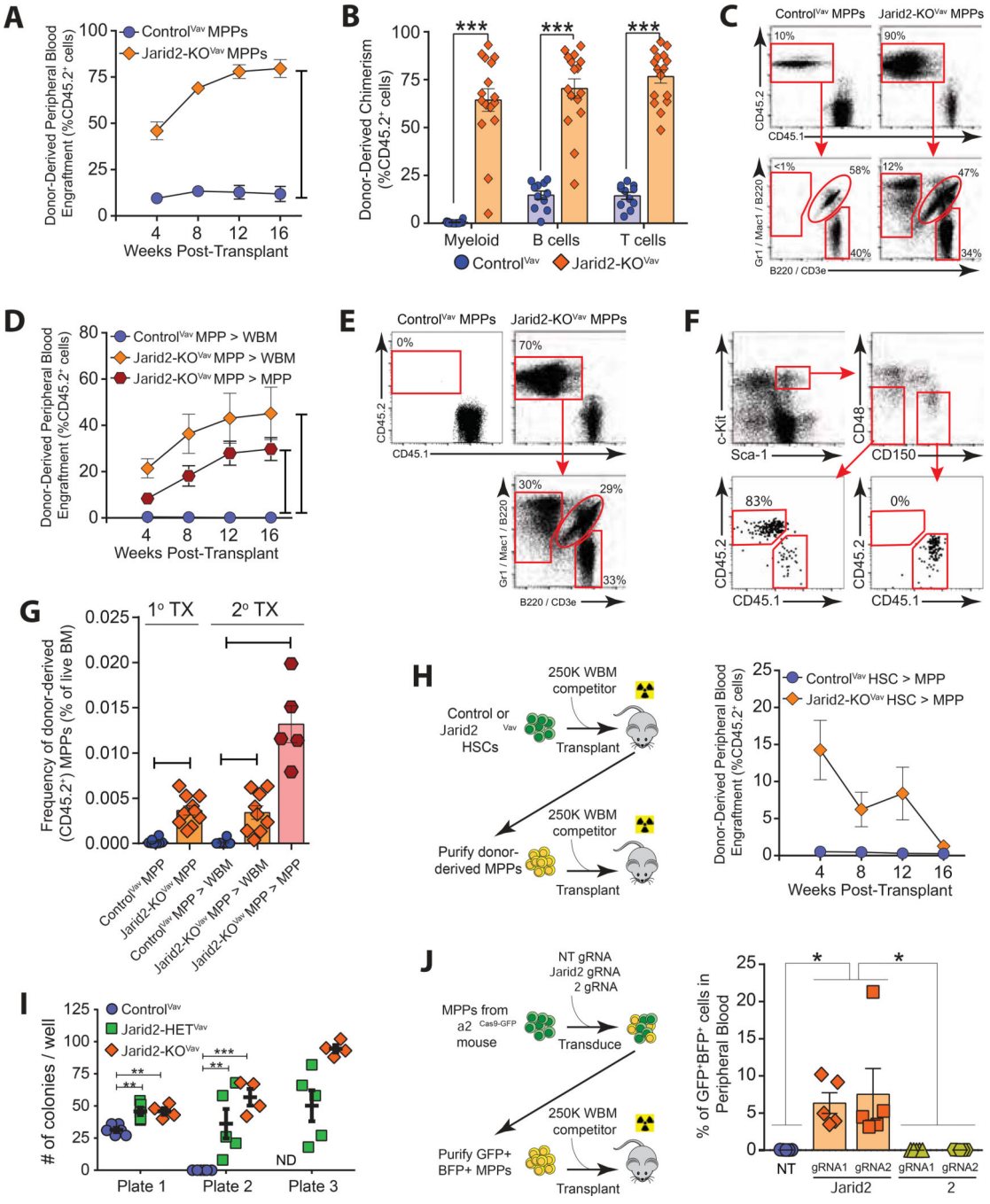

Figure 4: JARID2 Restricts Self-Renewal in Multipotent Progenitors.

(A) Contribution of 100 purified Control^{Vav} (n=14) or *Jarid2*-KO^{Vav} (n=16) MPPs to primary recipient peripheral blood.

(B) Chimerism of donor MPP-derived cells in myeloid, B and T cell lineages in primary recipients at 16 weeks post-transplant.

(C) Flow cytometry plots showing blood lineage distribution of donor-derived cells in primary recipients transplanted with Control^{Vav} or *Jarid2*-KO^{Vav} MPPs at 16 weeks posttransplant.

(D) Peripheral blood engraftment in secondary recipients of purified MPPs or WBM isolated from primary recipients transplanted with Control^{Vav} or *Jarid2*-KO^{Vav} MPPs (n=5–15).
(E) Flow cytometry plots showing blood lineage distribution of donor-derived cells in secondary recipients transplanted with Control^{Vav} or *Jarid2*-KO^{Vav} MPPs at 16 weeks post-transplant.
(F) Representative flow cytometry plots of secondary recipients transplanted with *Jarid2*KO^{Vav} MPPs.
(G) Quantification of donor-derived MPPs (CD45.2^{+}Lineage^{-}c-Kit^{+}Sca-1^{+}CD48^{-}CD150^{-}) in the BM of recipients transplanted with Control^{Vav} or *Jarid2*-KO^{Vav} MPPs at 18 weeks posttransplant.
(H) Peripheral blood engraftment from MPPs isolated from primary recipients transplanted with Control^{Vav} or *Jarid2*-KO^{Vav} HSCs (n= 8–10).
(I) Colonies generated in Methocult serial replating. For plate 1, 100 MPPs were sorted from mice (n=4–6), then 1×10^{4} cells were plated for serial rounds. ND = not determined (insufficient cells).
(J) 12 week peripheral blood engraftment of Cas9-expressing MPPs (GFP^{+}) transduced with the indicated gRNAs (BFP^{+}).
*p<0.05, **p<0.01, ***p<0.001, ****p<0.0001. Mean ± S.E.M. values are shown. See also Figure S4.

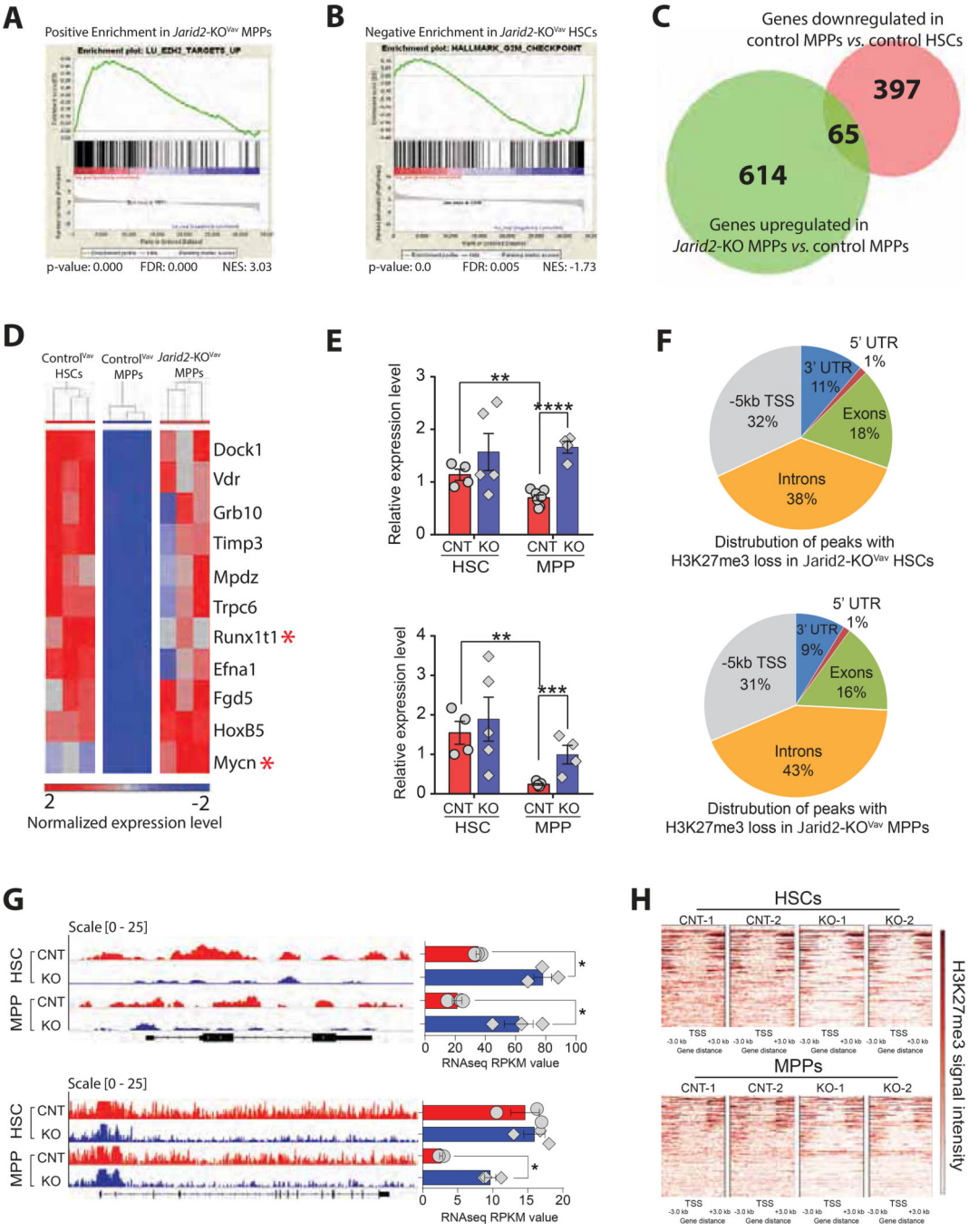

Figure 5: JARID2 Collaborates with PRC2 to Regulate Gene Networks that Govern HSC Identity.

(A) Gene Set Enrichment Analysis (GSEA) showing overlap of Ezh2 targets with genes upregulated in *Jarid2*-KO^{Vav} MPPs.

(B) GSEA showing negative enrichment of G_2/M checkpoint genes in *Jarid2*-KO^{Vav} HSCs.

(C) Overlap of genes downregulated in Control^{Vav} MPPs compared to Control^{Vav} HSCs, and those upregulated in *Jarid2*-KO^{Vav} MPPs compared to Control^{Vav} MPPs.

(D) Heatmap showing HSC "fingerprint" genes downregulated in Control^{Vav} MPPs that are de-repressed in *Jarid2*-KO^{Vav} MPPs.
(E) Expression levels of *Mycn* and *Runx1t1* in Control^{Vav} (CNT) and *Jarid2*-KO^{Vav} (KO) HSCs and MPPs by independent real-time PCR (n=4–6).
(F) Genomic distribution of H3K27me3 peaks lost in *Jarid2*-KO^{Vav} HSCs and MPPs compared to control counterparts.
(G) H3K27me3 profiles (left) and RNA-seq expression values (right) of *Mycn* (top) and *Runx1t1* (bottom).
(H) H3K27me3 profiles 3 kb upstream and downstream of transcriptional start sites (TSS).
*p<0.05, **p<0.01, ***p<0.001, ****p<0.0001. Mean ± S.E.M. values are shown. See also Figure S5 and Table S1.

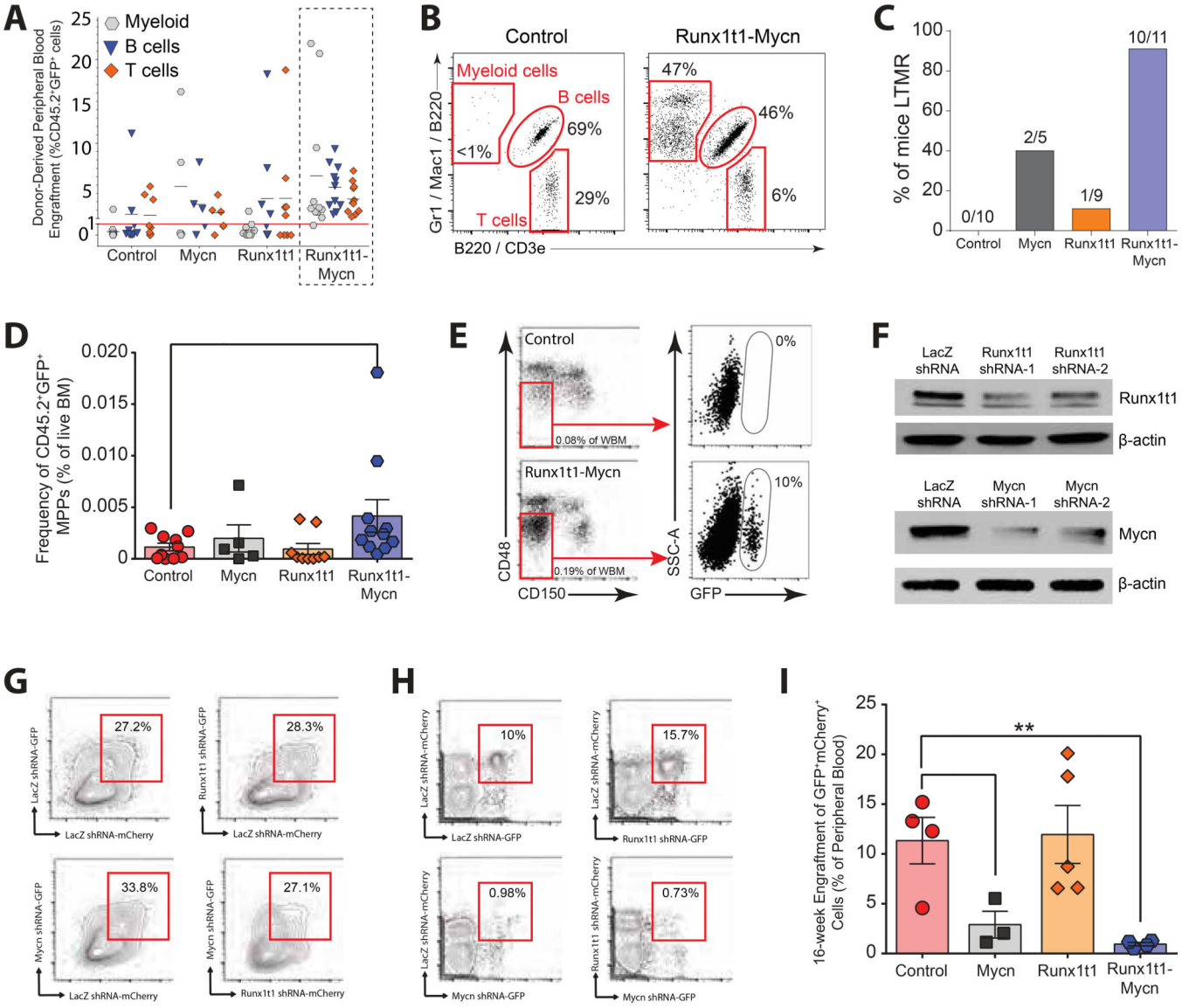

Figure 6: Mycn and Runx1t1 Co-expression Endows MPPs with Self-Renewal Potential.

(A) Contribution of transduced MPPs to hematopoietic lineages at 16 weeks posttransplantation (n=5–11).

(B) Flow cytometry plots showing lineage differentiation of transduced wild-type MPPs.

(C) Percent of recipient mice transplanted with transduced wild-type MPPs classified as long-term multi-lineage reconstituted (LTMR) at 16 weeks post-secondary transplant.

(D) Quantification of donor-derived MPPs ($CD45.2^+GFP^+Lineage^-c\text{-}Kit^+Sca\text{-}1^+CD48^-CD150^-$) in recipients transplanted with transduced wild-type MPPs 18 weeks post-secondary transplantation (n=5–11).

(E) Representative flow cytometry plots showing GFP^+ MPPs in the BM of recipients transplanted with transduced wild-type MPPs.

(F) Western blot of 32D cells transduced with shRNAs targeting LacZ, Runx1t1, and Mycn.

(G) Transduction efficiency of $Lineage^-c\text{-}Kit^+Sca\text{-}1^+$ cells from *Jarid2*-KO^{Vav} mice transduced with lentiviral shRNAs targeting LacZ, Mycn and/or Runx1t1.

(H) Representative flow cytometry plots showing percent of cells expressing shRNAs targeting LacZ, Mycn and/or Runx1t1 in blood of recipient mice.
(I) Percent of blood cells in mice transplanted with *Jarid2*-KO^{Vav} MPPs expressing shRNAs at 16 weeks post-transplant (n=3–5).
*p<0.05, **p<0.01. Mean ± S.E.M. values are shown. See also Figure S6.

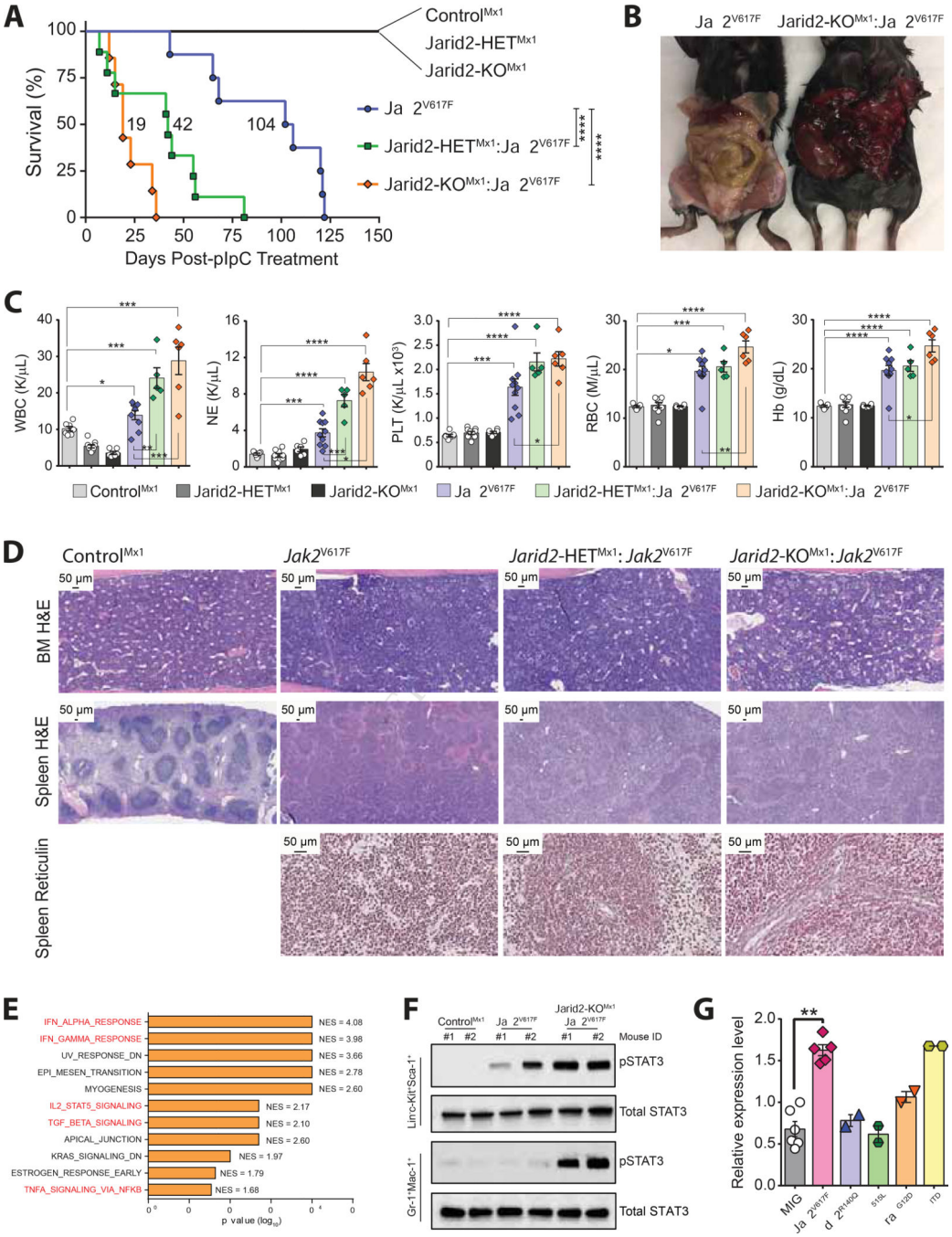

Figure 7: JARID2 Regulates Overlapping Mechanisms in Normal and Malignant Hematopoiesis.

(A) Kaplan-Meier plot comparing survival of Control^{Mx1} (n=7), *Jarid2*-HET^{Mx1} (n=6), *Jarid2*-KO^{Mx1} (n=6), *Jak2*^{V617F} (n=8), *Jarid2*-HET^{Mx1}:*Jak2*^{V617F} (n=9) and *Jarid2*-KO^{Mx1}:*Jak2*^{V617F} (n=7) mice after pIpC.

(B) Necropsy showing splanchnic vein thrombosis in abdominal cavity of a *Jarid2*KOMx1:*Jak2*V617F mouse.

(C) Blood counts from moribund animals.

(D) Histological analysis of moribund mice.

(E) GSEA analysis of *Jarid2*-KO^{Mx1}:*Jak2*^{V617F} HSCs compared to *Jak2*^{V617F} HSCs.
(F) Western blot of Lineage^{-}c-Kit^{+}Sca-1^{+} cells, and myeloid cells (Gr-1^{+}Mac-1^{+}) stimulated with IL-6.
(G) Normalized expression of *Jarid2* in Lineage^{-}c-Kit^{+}Sca-1^{+} cells 48 hr after induction of indicated mutations (n=2–5).
In C, values from *Jak2*^{V617F}, *Jarid2*-HET^{Mx1}:*Jak2*^{V617F} and *Jarid2*-KO^{Mx1}:*Jak2*^{V617F} mice are from moribund animals, whereas Control^{Mx1}, *Jarid2*-HET^{Mx1} and *Jarid2*-KO^{Mx1} values are taken from mice 150-days post-pIpC treatment. *p<0.05, **p<0.01, ***p<0.001, ****p<0.0001. Mean ± S.E.M. values are shown. See also Figure S7 and Tables S2 and S3.

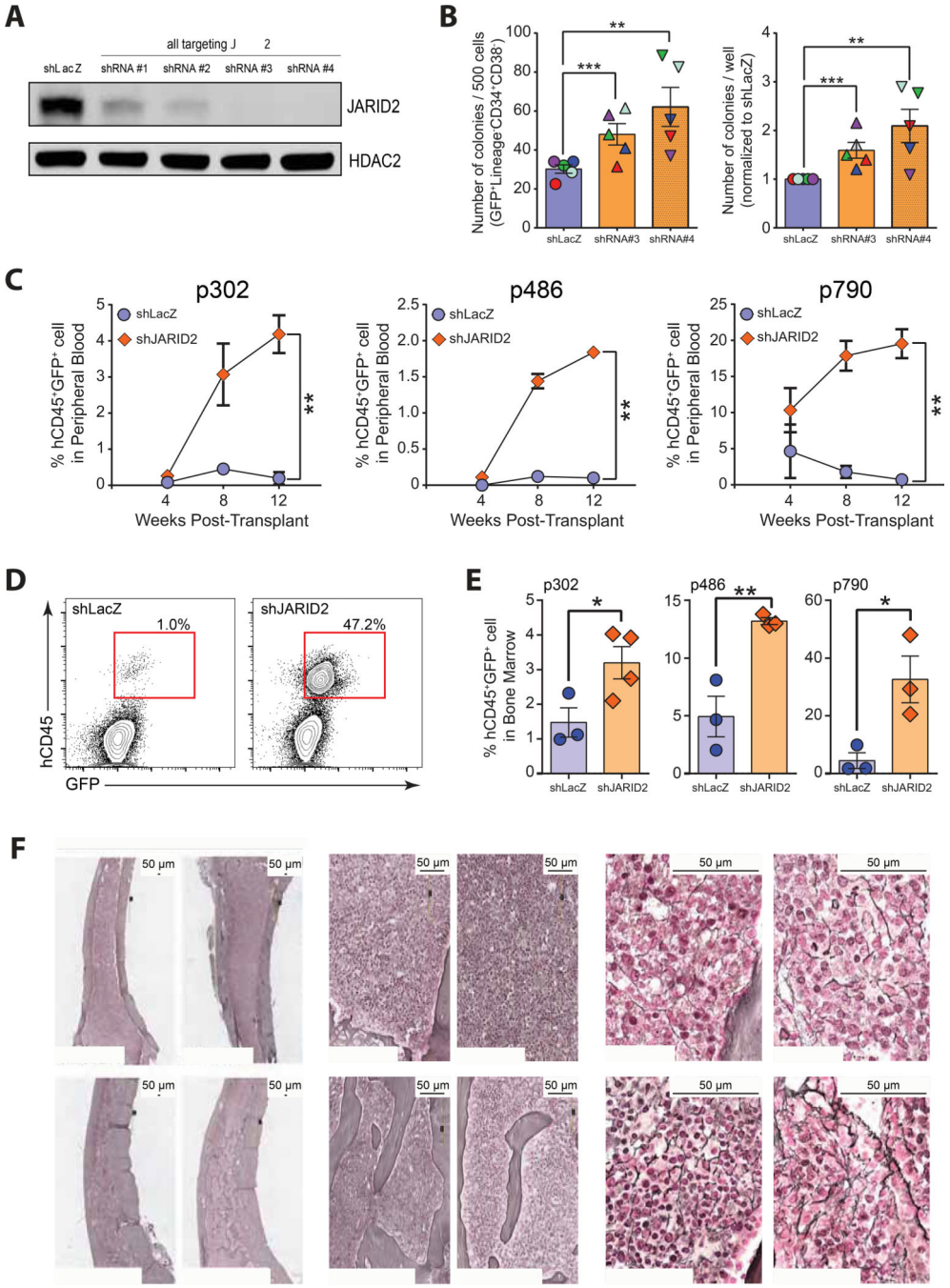

Figure 8: Inhibition of JARID2 in MPN Patient-Derived Cells.

(A) Protein levels of JARID2 in HEL cells transduced with indicated shRNAs.

(B) Colony formation from 500 Lineage^{-}CD34^{+}CD38^{-} cells from MF patients transduced with indicated shRNAs. Different colors represent samples from individual patients. Relative colony numbers are normalized to the LacZ control shRNA for each patient.

(C) Blood engraftment of MF CD34^{+} cells from individual patients transduced with indicated shRNAs in NSGS mice.

(D) Flow cytometry plots showing BM engraftment of MF $CD34^+$ cells transduced with indicated shRNAs at 12 weeks post-transplant.
(E) BM engraftment of MF $CD34^+$ cells from individual patients transduced with indicated shRNAs 12 weeks post-transplant.
(F) Reticulin staining of BM sections from NSGS mice transplanted with p790 $CD34^+$ cells transduced with indicated shRNAs. Red arrows indicate osteopetrotic trabecular bone formation.
*p<0.05, **p<0.01, ***p<0.001. Mean ± S.E.M. values are shown. See also Figure S8 and Table S4.